



**DEVELOPMENT OF A CONTINUOUS ION EXCHANGE PROCESS FOR
RECYCLING OF BATTERY METALS**

Lappeenranta–Lahti University of Technology LUT

Master's Program in Chemical Engineering

Master's Thesis

2023

Siiri Asumalahti

Examiners: D.Sc. Sami Virolainen

Prof. Tuomo Sainio

ABSTRACT

Lappeenranta–Lahti University of Technology LUT

LUT School of Engineering Science

Chemical Engineering

Siiri Asumalahti

Development of a continuous ion exchange process for recycling of battery metals

Master's Thesis

2023

79 pages, 42 Figures, 27 Tables and 1 appendix

Keywords: battery metals, lithium-ion battery, ion exchange, simulated moving bed, SMB, recycling, hydrometallurgy, cobalt, lithium, nickel, TP260 resin, MDS TP260 resin

Examiners: D.Sc. Sami Virolainen

Prof. Tuomo Sainio

The demand for Li-ion batteries is growing continuously and rapidly. The transition to electric vehicles and the increasing production of devices like laptops and mobile phones continuously increase the Li-ion battery demand. The batteries contain many metals, the most valuable of which are lithium, cobalt and nickel.

The goal of this Thesis was to develop a continuous ion exchange process to separate lithium, cobalt and nickel from LIB waste leachate, while minimizing their loss and maximizing the purity of the product. The continuous process was constructed utilizing a simulated moving bed (SMB) system.

To achieve this goal, 21 single column experiments and 3 SMB experiments were conducted. The SMB experiments gave good results, and each experiment was able to be significantly improved. The biggest challenge in the developed process was the amount of cobalt lost, but in the final process the achieved loss was very low in comparison to other battery recycling methods.

TIIVISTELMÄ

Lappeenrannan–Lahden teknillinen yliopisto LUT

LUTin insinööritieteiden tiedekunta

Kemiantekniikka

Siiri Asumalahti

Jatkuvatoimisen ioninvaihtoprosessin kehitys akkumetallien kierrätykseen

Kemiantekniikan diplomityö

2023

79 sivua, 43 kuvaa, 27 taulukkoa ja 1 liite

Avainsanat: akkumetallit, litiumioniakku, ioninvaihto, simulated moving bed, SMB, kierrätys, hydrometallurgia, kobaltti, litium, nikkeli, TP260 hartsit, MDS TP260 hartsit

Tarkastajat: D.Sc. Sami Virolainen

Prof. Tuomo Sainio

Litiumioniakkujen kysyntä nousee nopeasti ja jatkuvasti. Siirtymä sähköajoneuvoihin ja pienlaitteiden kuten puhelinten ja tietokoneiden kasvava valmistusmäärä lisää niiden kysyntää. Litiumionit sisältävät monia metalleja, joista arvokkaimmat ovat litium, kobaltti ja nikkeli.

Tämän diplomityön tavoite oli kehittää jatkuvatoiminen ioninvaihtoprosessi litiumin, kobaltin ja nikkelin erotukseen litiumioniakkujen jättemateriaalista, samalla minimoiden tavoitemetallien menetyksen ja maksimoiden tuotteen puhtauden. Jatkuva prosessi rakennettiin hyödyntämällä simulated moving bed (SMB) systeemiä.

Tämän tavoitteen saavuttamiseksi toteutettiin 21 yhden kolonnin koetta ja 3 SMB koetta. SMB kokeista saadut tulokset olivat hyviä, ja niitä pystyttiin parantamaan huomattavasti jokaisen kokeen välillä. Kehitetyn prosessin suurin haaste oli kobaltin menetys, mutta lopullisissa prosesseissa saavutettu menetys oli hyvin pieni muihin akkukierrätystapoihin verrattuna.

ACKNOWLEDGEMENTS

This Master's Thesis was a part of the BATix project funded by Metallinjalostajat fund (Metallinjalostajat ry.). This Thesis was done in the Department of Chemical Engineering at Lappeenranta-Lahti University of Technology LUT between November 2022 and August 2023.

I would like to thank the examiners, Sami Virolainen and Tuomo Sainio for their support, ideas and help with this work. There were times when I felt there was not path forward, but their expertise and great advice always kept me going.

I also want to thank Tobias Wesselborg for his invaluable contributions during this process. From the minute details to large concepts, I could always rely on his help and ideas.

I also thank my friends and family for their support during this process.

Failure is never an option!

Contents

ACKNOWLEDGEMENTS	4
1 INTRODUCTION	7
2 RECYCLING OF BATTERY METALS	10
2.1 Composition of Li-ion batteries	10
2.2 Current recycling methods of batteries	11
3 ION EXCHANGE	13
3.1 Materials used in ion exchange	16
3.1.1 Lewatit TP260 and Lewatit MDS TP260 Resin.....	17
3.3 Applications of ion exchange	19
4 SIMULATED MOVING BED SYSTEMS	20
4.1 Working principle of the SMB	20
4.2 SMB applications	22
5 LABORATORY EXPERIMENTS	22
6 SINGLE COLUMN EXPERIMENTS	23
6.1 LIWBL single column experiment	26
6.1.1 LIWBL single column experiment results	27
6.1.2 Recoveries of metals in LIWBL single column experiment	31
6.2 Fe desorption experiments	32
6.2.1 Fe desorption experiments results	33
6.3 Washing 1 M H₂SO₄ with raffinate	36
6.4 Single column experiment with SMB switch times using TP260 resin	37
6.4.1 Single column experiment with SMB switch times using TP260 resin experiment results	39
6.4.2 Single column experiment with SMB switch times using TP260 resin and 50 % diluted metal solution experiment results.....	41
6.5 Single column experiment with SMB switch times using MDS TP260 resin	44
6.5.1 Single column experiment with SMB switch times using MDS TP260 resin experiment results	45
6.5.2 Single column experiment with SMB switch times using MDS TP260 resin and 50 % diluted metal solution experiment results.....	48
6.5.3 Single column experiment with SMB switch times using MDS TP260 resin metal recoveries and losses	51
6.6 Conclusions of the single column experiments	52
7 CONSTRUCTION OF THE SIMULATED MOVING BED SYSTEM	54

8 SIMULATED MOVING BED EXPERIMENTS	58
8.1 SMB 1	58
8.2.1 SMB 1 results.....	59
8.2 SMB 2	63
8.2.1 SMB 2 results.....	64
8.3 SMB 3	67
8.3.1 SMB 3 results.....	68
8.4 Discussion regarding the SMB experiments	72
9 CONCLUSIONS	73
REFERENCES	74
APPENDICES	79

1 INTRODUCTION

Currently, we are not only living through a climate crisis, but also a waste crisis. There are massive problems with landfill waste, toxic materials leaching into the ground and ultimately in our water sources. These toxic materials can gravely harm nature's ecosystems, wildlife and even humans, especially in developing countries.

Li-ion batteries power up our smartphones, computers and even cars, and in 2016 they demanded a 35 % global market share for all lithium usage. (Guiral 2018) The share is growing because of electric vehicles which all demand Li-ion batteries. Battery demand for electric vehicles increased 65 % from 2021 to 2022. (IEA 2023 a) From 2017 to 2022 the global trend caused a 40 % increase in nickel demand, 70 % increase in cobalt demand and tripled lithium demand. (IEA 2023 b)

All these Li-ion batteries use a lot of critical raw materials. Lithium, for example, is on EU's endangered raw materials list, since it has serious availability issues. Another main component of Li-ion batteries, cobalt, is also on EU's critical raw materials list. (European Commission 2023) Cobalt's top producer globally is the Democratic Republic of Congo, and the production has been reported to result in bad and unsafe working conditions, child labor, and water, air, and soil pollution. These issues can lead to decreased crop, contaminated food and water, and respiratory and reproductive health issues for locals. (Earth Org 2023)

These critical materials that Li-ion batteries consist of can be recycled from secondary sources, for example, used Li-ion batteries. Developing a profitable and a sustainable way to recycle the used batteries is essential for our future, on a global scale.

The current battery recycle methods have a few main issues; they're costly, the yield of the recycled battery metals is not great, and their productivity is low. The battery recycling method that is researched in this Thesis is ion exchange implemented in a simulated moving bed column system.

Ion exchange is an efficient battery metals recycling method, since it allows for the better purification and recovery efficiency of valuable battery metals compared to for example more conventional hydrometallurgical separation methods solvent extraction and precipitation (Virolainen, Wesselborg, Sainio 2021), including previously mentioned lithium and cobalt. During the ion exchange process, the ions of the metals are exchanged with other ions in a solution, allowing for the selective separation and recovery of the desired metals.

When compared to other battery recycling methods, like smelting, which involve high temperatures and lead to harmful emissions, ion exchange is more clean and more environmentally friendly process. It also can be performed at a smaller scale which makes it more accessible for smaller operations. In smelting, one of the most valuable metals, lithium, is lost to the slag fraction, which would not happen in ion exchange.

The ion exchange processes in industrial hydrometallurgy are typically done as single column, or lead-lag, batch-type processes (Sole et al 2016 a), but a continuous process can be developed utilizing the simulated moving bed system. Continuous processing involves a continuous flow of material through the recycling process, as opposed to batch processing where the material is processed in discrete batches. Continuous processing can offer advantages such as higher throughput, reduced energy consumption, and lower labor costs.

The metals that Li-ion batteries typically consist of are lithium, cobalt, iron, aluminum, copper, nickel, and manganese. The goal in this Thesis is to implement ion exchange in a simulated moving bed column system since it can result in a continuous battery recycling process, which is more environmentally friendly, efficient, and better purification and recovery.

The main questions of the Thesis are:

- I. What are the optimal parameters for ion exchange process for recovery of lithium, cobalt and nickel from Li-ion battery waste?

II. How to construct a simulated moving bed system combined with the optimal ion exchange process?

III. Is the constructed simulated moving bed ion exchange Li-ion battery recycling method better than a traditional batch process?

2 RECYCLING OF BATTERY METALS

2.1 Composition of Li-ion batteries

All batteries, or energy storage systems (ESS), are divided into five categories: mechanical, electrochemical, chemical, electrical and hybrid systems. Li-ion batteries are classified into electrochemical storage systems. Li-ion batteries have been used commercially since 1991, and since then their use has increased exponentially with the explosive growth of cellphones, cameras, power tools, and other electronics. (Singh 2019)

In 2016, li-ion batteries had a market share of more than 90 % out of all battery types. (Rietveld 2019) Li-ion batteries consist of several metals; cobalt, nickel, lithium, copper, manganese, iron, and aluminium. (Sobianowska-Turek 2021)

A Li-ion battery consists of a cathode, which is positively charged, an anode, which is negatively charged, positive and negative current collectors, separator, and electrolyte. While charging the battery by connecting it to an electric current, the lithium ions are released from the cathode to the anode. After the battery has been charged, and the electricity stored in it needs to be used, the lithium ions travel from the anode back to the cathode. After the electricity has been used, the battery can be charged and used again. (Chawla 2019) The working principle of a Li-ion battery is presented in Figure 1.

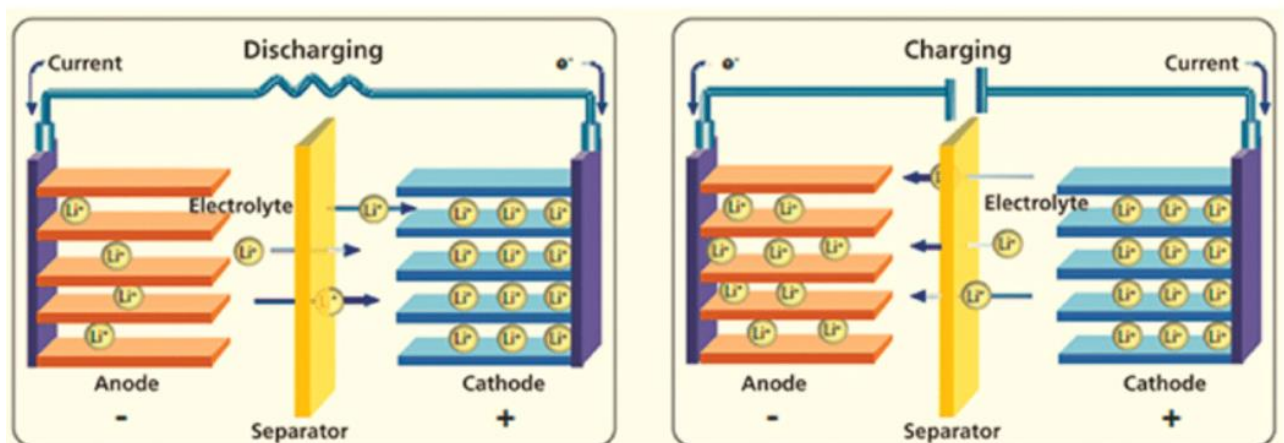


Figure 1 Working principle of a Li-ion battery (Chawla 2019)

The most expensive LIB metals are lithium, nickel and cobalt. These metals are the ones that will be the most focused on to separate when developing the continuous ion exchange process. These metals are of interest in any type of battery recycling process, so the process developed in this Thesis is no exception. Their market values have fluctuated significantly since 2017, as can be seen in Figure 2. In the start of 2023, lithium's price had nearly quintupled, nickel's tripled and cobalt's also increased. (IEA 2023 a)

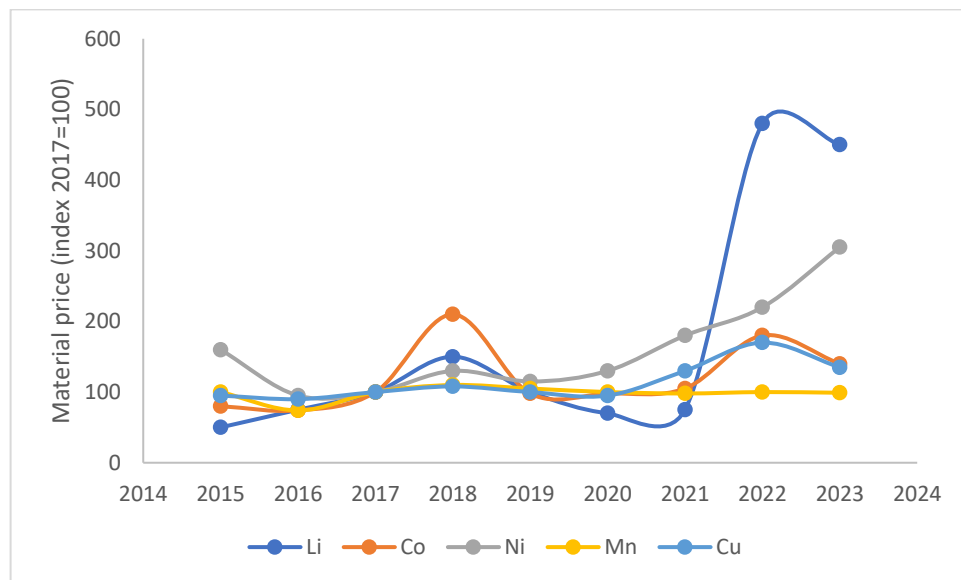


Figure 2 Market prices of lithium, cobalt, nickel, manganese, and copper (index 2017=0) (IEA 2023 a)

2.2 Current recycling methods of batteries

Li-ion batteries can be currently recycled multiple ways, which include three process types: pyrometallurgy, hydrometallurgy and direct recycling. (Baum 2022)

Direct recycling separates the components of the battery manually and cathode material can be reused in batteries or other application with minimal additional treatment. This method, however, does not allow for the recovery of separated metals.

Hydrometallurgical processes in Li-ion battery recycling result in a Li-ion battery waste leachate (LIBWL), which contains all the LIB metals together in a aqueous solution. With further processes, like the ones that are studied in this Thesis, separation of valuable metals

such as cobalt, nickel and lithium can be achieved. (Porvali 2019) The metal content in Li-ion battery waste leachate is presented in Table I.

Table I Concentrations of metals in Li-ion battery waste leachate (Porvali 2019)

Metal	Concentration, mg/L
Ni	1996
Li	2548
Co	16817
Cu	2145
Mn	2146
Fe	741
Al	1519

Hydrometallurgical processes include leaching, which can utilize several acids, including hydrochloric, nitric and sulphuric acid as leachants. The use of different leachants can vary this process greatly, and cobalt recovery can vary from 40 % to 92 %. Especially the increase of hydrogen peroxide in the process promotes cobalt recovery by reducing Co(III) to Co(II). (Chagnes, Pospiech 2013)

The separation of metals from the leachate can be achieved using solvent extraction. Solvent extraction as a process is simple, and therefore easy to industrialize. It can recover 90 % of cobalt and 90 % of nickel. (Tang et al 2023)

Another way of separating metals from leachate is precipitation. The metals can be precipitated from the leachate as microparticles by adding ammonium oxalate. This method can recover 71 % of lithium and 94.7 % of cobalt. (Zhu et al 2012)

Pyrometallurgical processes result also in a mix of metals, but because of the high temperatures, metals such as aluminium and lithium oxidize during the process and can not be recovered from the waste. With further hydrometallurgical processes, metals can also be separated from the pyrometallurgical recycling product, but it does not contain all of the metals in a Li-ion battery, including lithium, which is among the most valuable. (U.S. Department of Energy Office of Scientific and Technical Information 2023)

Some of the largest global battery recycling companies are presented in Table II.

Table II Large global battery recycling companies

Company	Location
Umicore	Belgium
Ecobat	USA
EnerSys	USA
Glencore	Switzerland
RecycLiCo	Canada
Li-Cycle	Canada
Ganfeng Lithium Group	China
Exide Industries	India

Companies like RecycLiCo use hydrometallurgical methods of recycling (RecycLiCo 2023) and some companies like Ecobat, also use physical recycling methods (Electrive 2023)

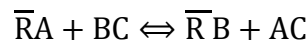
Some companies use a combination of recycling methods, like Umicore, which combines pyro- and hydrometallurgy in their processes. (Umicore 2023)

Recycling plants that use only hydrometallurgy are rare, but prominent ones include France based Recupyl and Retrie, which is based in the United States and Canada. (Larouche et al 2020)

3 ION EXCHANGE

In an ion exchange reaction, ions in liquid phase exchange places with the ions present in the solid phase on the surface of ion exchange materials. The liquid phase ions exist in the electrolyte solution fed through ion exchange material, which contain exchangeable cations or anions, depending on the type of the ion exchange material. (Nasef 2012)

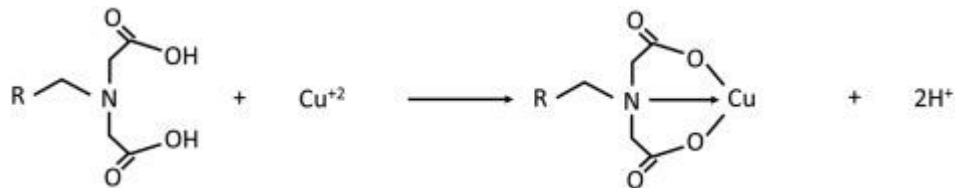
Ion exchange is an equilibrium-controlled process, which means that the change of the liquid phase ions and the exchangeable cations and anions until an equilibrium is reached. The ion exchange equilibrium equation is presented below.



In which, A counter ions
 B counter cations
 C co-ions

There are several other ion exchange equilibrium reactions and they can be divided into several subcategories. The reaction that is used in the ion exchange in the process in this thesis is chelating. Chelate ion exchangers have a high selectivity for heavy metals. (Yoshida et al 1985)

The chelating reaction using copper ion as an example is presented below. (Barbosa Botelho et al 2019)



The ion exchange equilibrium process is presented in Figure 3. Ion exchange materials have a limited number of exchangeable ions, and when equilibrium is reached, ion exchange is no longer possible. At this point, the particles that attached to the material are removed and the material is regenerated for new ion exchange. The ion exchange material must always be in zero-charged state, particles are always attached to it, but the particles can get replaced with another particle with higher affinity. Only one particle can attach to an active site. (Ramkumar 2012)

Ion exchange process is highly dependent on the pH of the process, the process efficiency increasing when the pH increases. This is due to the fact that increasing the pH decreases the H^+ concentration. H^+ competes with the metal ions for the active site in the ion exchange resin, so when their number decrease, the number of metal ions that can attach to the resin increase, resulting in more efficient adsorption. (Barbosa Botelho et al 2019)

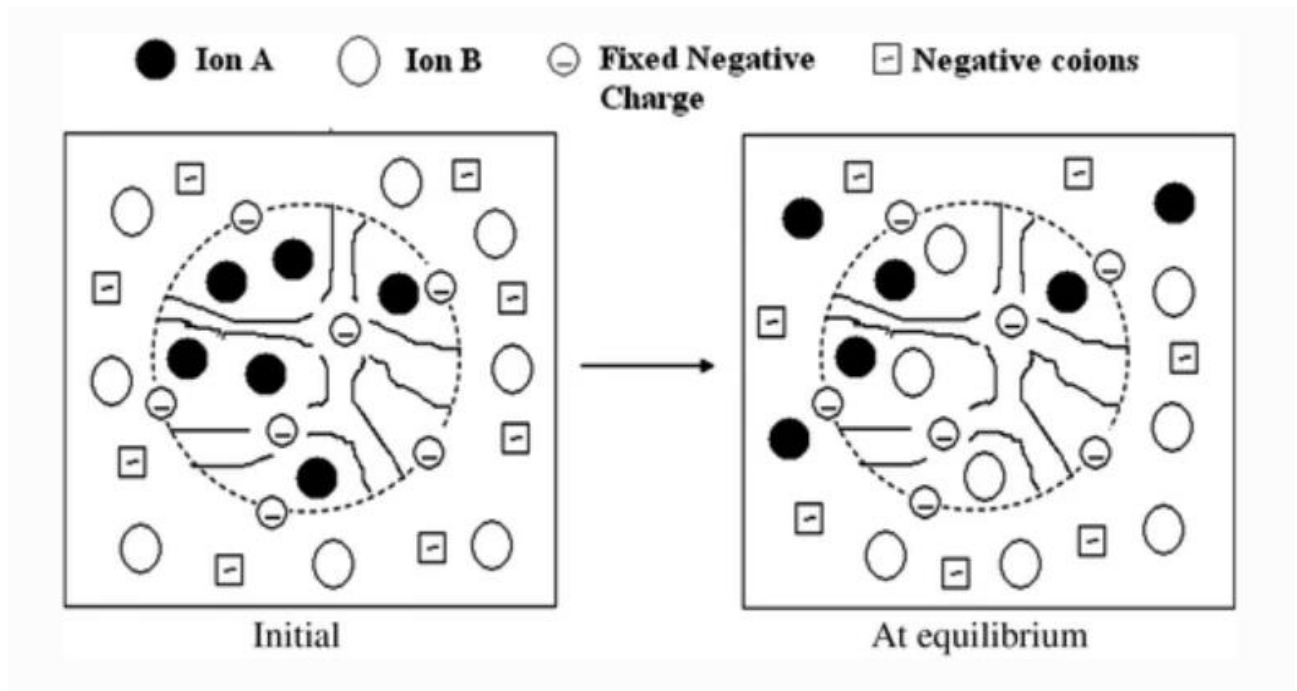


Figure 3 Ion exchange equilibrium process (Ramkumar 2012)

The separation of metals by ion exchange is based on the different affinities of the metals to a specific ion exchange material. This causes the metals with the higher affinities to use up most of the active sites in the ion exchange material. If a metal with lower affinity has used up an active site, a metal with higher affinity can replace it. (Toumi et al 2007)

In the separation of battery metals with the Lewatit TP260 resin, the metals fall in to three different groups in the basis of their affinity. The largest affinity is with iron and aluminium, which are recovered last in the ion exchange. The second largest affinity is with copper and manganese, which are recovered from the ion exchange column after the group which has the least affinity, cobalt, nickel and lithium. The metals with smaller affinities travel through the ion exchange material faster, making it possible to collect a product with only the desired metals until the undesired metals break through the column. (Virolainen, Sainio, Wesselborg 2021)

3.1 Materials used in ion exchange

Ion exchangers are a class of materials which are held together by chemical bonds, polyions, and allow for the movement of oppositely charged ions and can be replaced by similarly charged ions. Parameters related to the ion exchange material like type of functional groups and the physical form, for example, size of the material can affect the overall success of the ion exchange.

Ion exchange materials can generally be minerallic or inorganic and the vast majority of the inorganic are synthetic polymers. These polymers are available in anionic and cationic forms, but minerallic materials such as zeolites only exist in cation form only.

In addition to minerallic and inorganic materials, organic ion exchange materials can be anionic, cationic or amphoteric, which is a combination of anionic and cationic. (Nasef 2012)

The ion exchange materials used in the experiments of this Thesis, are inorganic synthetic polymers in cationic form, Lewatit TP260 and Lewatit TP260 MDS.

Some commonly used inorganic ion exchange materials and their polymeric structure are presented in Figure 4.

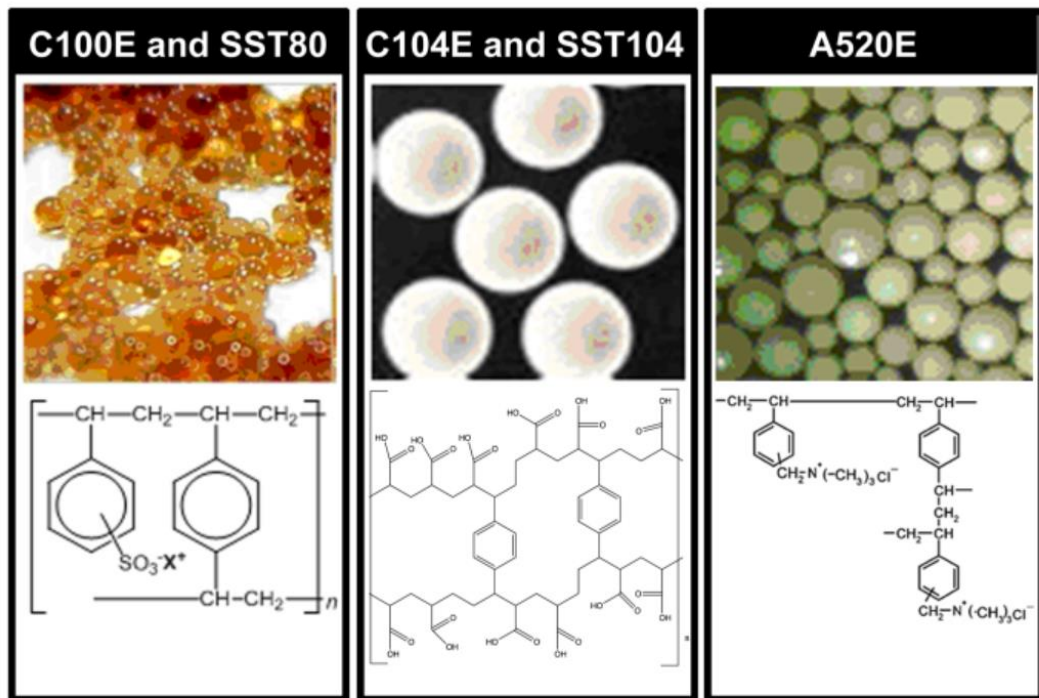


Figure 4 Chemical formula and physical features of some inorganic ion exchange material (Domenech et al 2012)

3.1.1 Lewatit TP260 and Lewatit MDS TP260 Resin

A resin that was used in the experiments in this Thesis is Lewatit TP260 resin. The parameters of Lewatit TP260 are presented in Table III. It is weakly acidic and macroporous cation exchange resin. Its bead size range is 0,4-1,25 mm and the volume change can be up to 25 % which can cause shrinking in the column. The functional group of both TP260 and MDS TP260 is aminomethylphosphonic acid. The chelating amino methyl phosphonic acid groups are designed for the selective removal of heavy metal cations.

TP260 works well in removal of heavy metals, especially copper and aluminium. It has difficulties in desorption of iron in its trivalent stage, which is why it is necessary to use a

two-step desorption of sulphuric acid and oxalic acid in order to desorb the iron and aluminium from the start of the column where they get stuck when fed to the column.

TP260 has a maximum operating temperature of 80 °C and pH range of 1-12, which are well within the operating range of the experiments. The resin can also be operated over numerous loading cycles, so it will work well in the continuous ion exchange process where the resin is continuously regenerated. (Lenntech 2019 a)

Table III Properties of aminomethylphosphonic acid -functional Lewatit TP260 ion exchange resin. (Lenntech 2019 a)

Maximum operating temperature, °C	80
pH range, -	1-12
Matrix	Crosslinked polystyrene
Functional group	Aminomethylphosphonic acid
Bead size range, mm	0,4-1,25
Water retention, m-%	58-62
Volume change, vol-%	25

MDS TP260 Resin, which differs from TP260 physically by its smaller bead size, was also used in the experiments of this Thesis. Due to its smaller size, it can lead to less leakages and up to 100 % higher operating capacity of metal separation than the standard TP260. (Lenntech 2019 b)

The parameters of MDS TP260 Resin are presented in Table IV.

Table IV Properties of aminomethylphosphonic acid -functional Lewatit MDS TP260 ion exchange resin (Lenntech 2019 b)

maximum operating temperature, °C	80
pH range, -	1-12
Matrix	Crosslinked polystyrene
Functional group	Aminomethylphosphonic acid
Mean bead size, mm	0.40
Water retention, m-%	63
Volume change, vol-%	35

3.3 Applications of ion exchange

Ion exchange reactions and resins have been used combined with a simulated moving bed process in the sugar processing industry for the past 35 years. Some of the applications included are desugaring of molasses and the separation of fructose from mixed sugars in order to produce high-fructose corn syrup, which is commonly used in consumer goods in the USA. (Silva et al 2012)

Ion exchange applications are widely used in metal removal and separation. Metal separation with ion exchange is possible with their different affinities to ion exchange materials. This allows for the separation of few metals from other when treating a metal mixture with ion exchange. Parameters such as solution pH, type of ion exchanger material and contact time with the material affect these processes greatly. (Lopes et al 2012)

Ion exchange has multiple applications in hydrometallurgical processes. Ion exchange has been proven to be especially useful when the content of the target metal is low. It can be utilized in several different type of processes like recovery, purification and separation. This means that when a product has low quantities of impurities, ion exchange is often the preferred method to remove those impurities. It can also be used to scavenge valuable metals from waste in which their contents are low, like recovering copper from mine waste streams. (Sole et al 2016 a)

Ion exchange has proven to work well for copper recovery from mine waste streams, since the content of copper in it is low, and the volume of the waste stream is high. Ion exchange is also capable of dealing with fluctuation of the content of the target metal in the

feed, which makes it a good option for waste streams, where the content is unreliable. The number of these applications used for industrial process waste are in the thousands. (Sole et al 2016 b)

Ion exchange has made possible to reduce nickel content from cobalt electrolytes from 900 mg/L to less than 160 mg/L in 40 g/L cobalt electrolytes. This reduction makes the cobalt more than 99.9 % pure. (Fleming et al 2003)

4 SIMULATED MOVING BED SYSTEMS

A simulated moving bed (SMB) is a system that combines the cross current flow of a liquid and a solid phase. It can be much more effective than a traditional fixed bed system when used in chromatography separation applications. With the SMB, it is possible to work a chromatography separation as a continuous process instead of a batch process.

SMB technology can provide a high separation rate, lower costs, lower resource use, better product yield and better efficiency. (Wang 2019)

4.1 Working principle of the SMB

In a traditional fixed bed system, a single column is charged with feed solution and then the column eluted, desorbed and regenerated before starting the process again. In a simulated moving bed system, the process is performed on multiple columns simultaneously, which are separated into zones, each column performing a different step of the process.

In an SMB, the fresh feed, elution, desorption and regeneration streams are entering the system simultaneously. This feed pattern is achieved by changing the inlet ports of the feed streams in tandem with the switch of the columns. (Rodrigues et al 2015)

The principle of the SMB is presented in Figure 5.

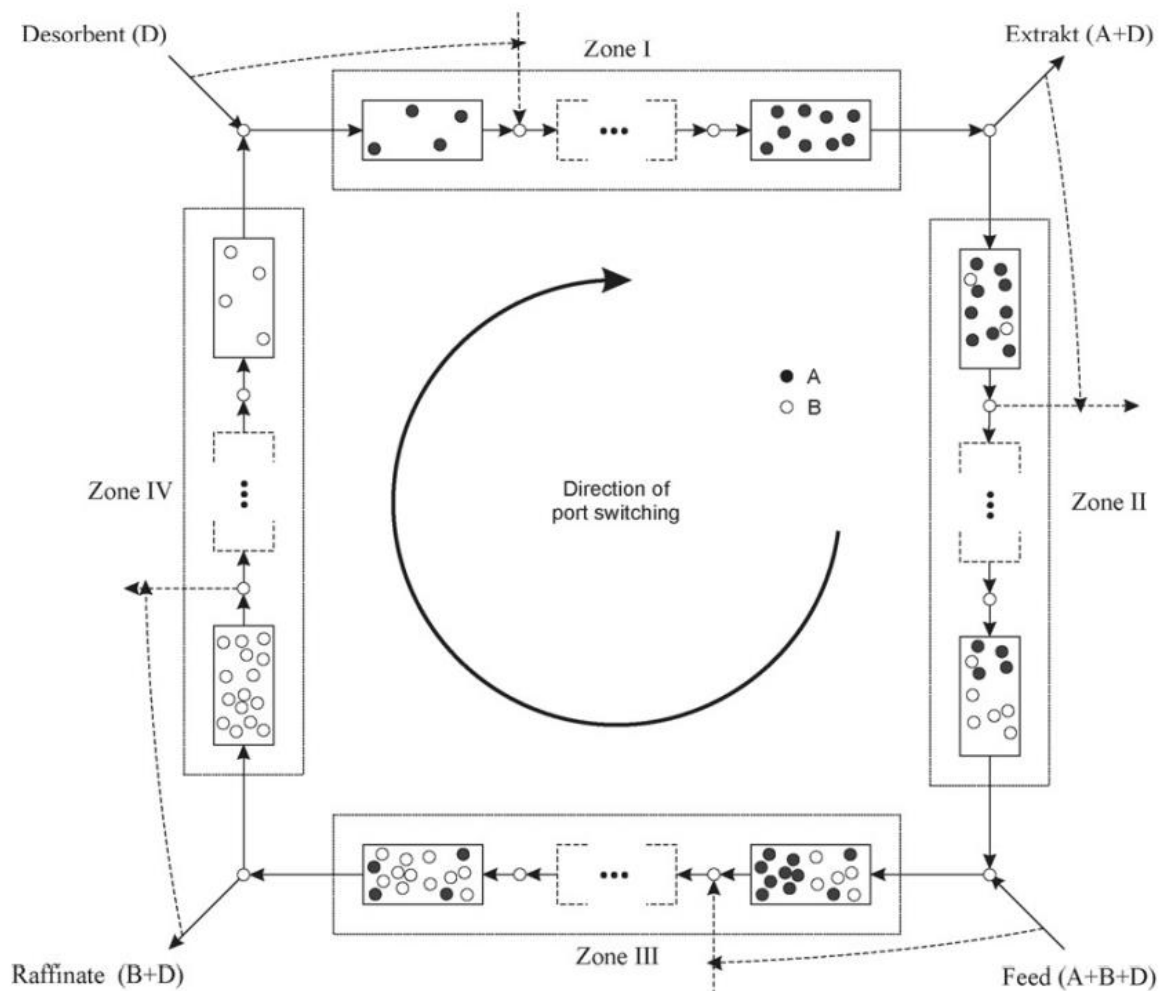


Figure 5 Working principle of the simulated moving bed system (Toumi et al 2007)

In Figure 5, the depicted SMB setup has four zones with two columns in each zone. In zones 1-4 it can be seen that the feed and desorbent are fed into the system and the outlets are raffinate and extract. As shown in the Figure, the outlet and inlet shift in between the columns, which causes the movement of the solid stream to be “simulated”. Out of the outlets, raffinate is the desired product and extract is the undesired separated compounds from the raffinate. In different applications of the SMB the number of inlets, outlets and their contents may vary. The zones can be connected or disconnected and have a different number of columns in them.

The SMB used in this Thesis works with a computer program and several motor valves that allow the outlet and inlet streams shift in between the columns, creating “switches”.

The switch is the time interval after which the feed and outlet locations are changed to other columns. Depending on the amount of columns in the SMB and the complexity of the process, the amount of switches can vary. When all the switches are completed, the SMB finishes a cycle, meaning that all of the columns in the SMB have gone through all the different process steps. Because of this structure, the columns don't need external desorption or regeneration and the SMB can operate continuously. (Rodrigues et al 2015)

4.2 SMB applications

Even though the SMB has been used in industrial applications since the 1960s, it has not been used in industrial scale applications of battery metals recycling, or even in hydrometallurgical ion exchange in general.

Industrial scale SMB applications are now used in biorefinery, petroleum and energy industries. SMB is also used in pharmaceutical technology. (PharmaTech 2007)

SMB technology works particularly well in biorefinery since it allows for an economically conscious solution for isolating the desired products from the mixture in biorefineries. In biorefineries, this step accounts for a large part of the costs of operating, but with using an SMB, it provides higher yield and lower desorbent usage, which both lower total costs. (Sharma 2021)

5 LABORATORY EXPERIMENTS

To conduct laboratory experiments for this Thesis, several different solutions were prepared. The experiments were based on a synthetic Li-ion battery waste leachate (LIBWL), which was prepared using cobalt, lithium, nickel, iron, aluminium, copper, and manganese.

The LIWBL solution was prepared using VWR NORMAPUR anhydrous Copper (II) sulphate, VWR RECTAPUR Nickel (II) sulphate hexahydrate, VWR RECTAPUR anhydrous Iron (III) sulphate, VWR Technical Cobalt (II) sulphate heptahydrate, ACROS

Lithium sulphate monohydrate, VWR NORMAPUR Manganese (II) sulphate monohydrate and ACROS Aluminium sulphate octadecahydrate to 0.85 M Na₂SO₄ using VWR RECTAPUR anhydrous sodium sulphate. The Solution was pH-balanced to pH 1,8 using VWR TECHNICAL 95 % sulphuric acid.

The 1 M H₂SO₄ used for desorption 1 and regeneration in the experiments, was prepared using VWR TECHNICAL 95 % sulphuric acid.

The 1.8 pH aqueous H₂SO₄ used for elution in the experiments was prepared using VWR TECHNICAL 95 % sulphuric acid.

The 0.4 M K₂-oxalate used for desorption 2 in the experiments was prepared using Scientific Potassium oxalate monohydrate.

The 741 mg/L Fe-solution used in the experiments was prepared using VWR RECTAPUR anhydrous Iron (III) sulphate and was pH-balanced to 1.8 using VWR TECHNICAL 95 % sulphuric acid.

All of the solutions were prepared by weighing the chemicals used in the solution to a beaker using an analytical scale (RADWAG AS 220.R2) or a laboratory scale (Precisa XB 4200 C) for a few higher weights and finishing the solution in a volumetric flask. The different solutions were prepared in 2 L, 1 L and 500 mL volumetric flasks.

The laboratory experiments for the Thesis consisted of twenty-one single column experiments and three simulated moving bed experiments.

The TP260 and TP260 MDS resin used in the experiments was used in protonated form and was preconditioned with acidic solution.

6 SINGLE COLUMN EXPERIMENTS

The laboratory experiments were performed using a multi metal solution that was made to synthetically represent Lithium-ion battery waste leachate (LIWBL). Single-column experiments C1-C19 were performed with columns filled with Lewatit TP260 resin, and experiments C20-C21 with Lewatit MDS TP260 resin. All single column experiments and their aims are presented in Table V.

Table V Aims and names of single column experiments performed for the Thesis.

Experiment	Aim
C1	First column experiment with very long switch times, multi metal solution feed for 8 BV (LIBWL)
C2	H ₂ SO ₄ removal from column with 0.7 Na ₂ SO ₄
C5	Fe-solution test, Fe feed for 0.5 BV, Elution with 0.2 M Na ₂ -oxalate
C6	Fe-solution test, Fe feed for 1 BV, Elution with 0.2 M Na ₂ -oxalate
C7	Fe-solution test, Fe feed for 1.5 BV, Elution with 0.2 M Na ₂ -oxalate
C8	Fe-solution test, Fe feed for 2.5 BV, Elution with 0.2 M Na ₂ -oxalate
C9	Fe-solution test, Fe feed for 2.5 BV, Elution with 0.4 M K ₂ -oxalate
C10	Fe-solution test, Fe feed for 4.5 BV, Elution with 0.2 M Na ₂ -oxalate
C11	Fe-solution test, Fe feed for 6 BV, Elution with 0.2 M Na ₂ -oxalate
C13	100 % metal solution experiment ("25 min switch times", i.e. volume flowrates are adjusted)
C14	50 % metal solution experiment ("25 min switch times", i.e. volume flowrates are adjusted)
C15	Fe-solution test, Fe feed for 0.5 BV, Elution with 0.4 M K ₂ -oxalate
C16	Fe-solution test, Fe feed for 1 BV, Elution with 0.4 M K ₂ -oxalate
C17	Fe-solution test, Fe feed for 1.5 BV, Elution with 0.4 M K ₂ -oxalate
C18	Fe-solution test, Fe feed for 4.5 BV, Elution with 0.4 M K ₂ -oxalate
C19	Fe-solution test, Fe feed for 6 BV, Elution with 0.4 M K ₂ -oxalate

	oxalate
C20	MDS TP20 100 % metal solution experiment ("25 min switch times", i.e. volume flowrates are adjusted)
C21	MDS TP260 50 % metal solution experiment ("25 min switch times", i.e. volume flowrates are adjusted)

The single column experiments were conducted on a test equipment setup that is shown in Figure 6.

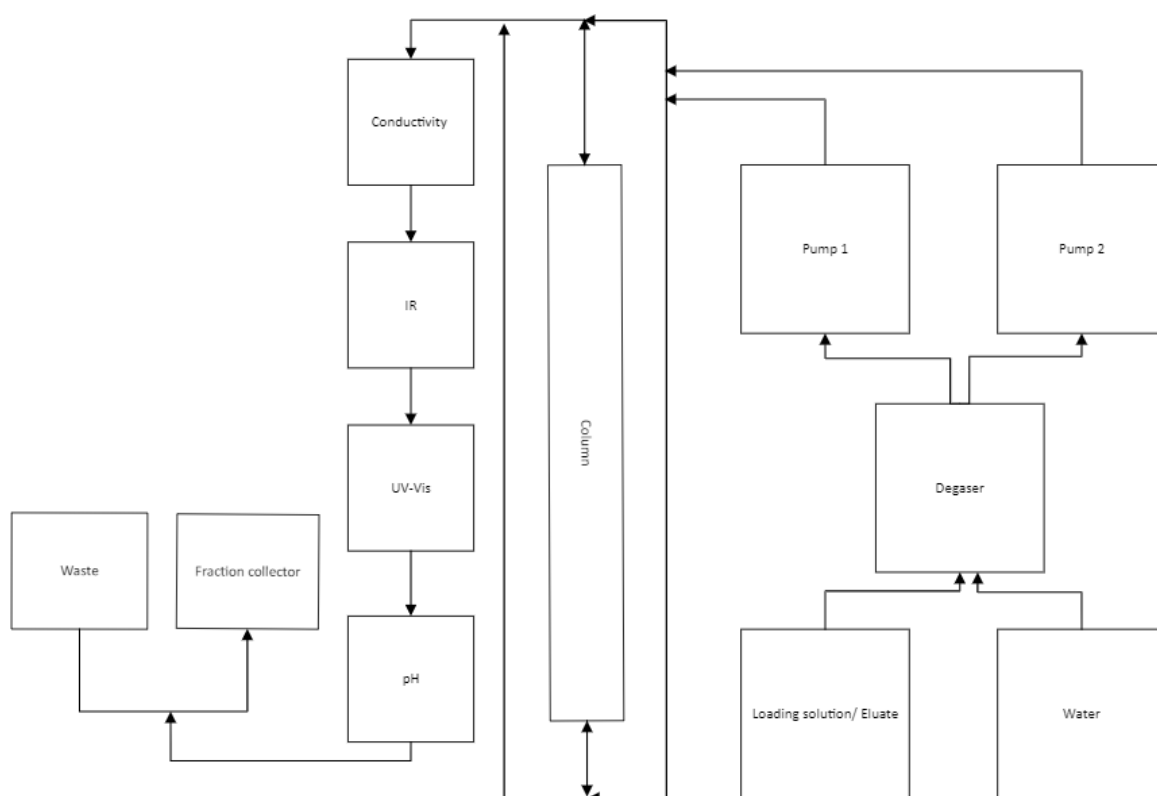


Figure 6 Flow diagram of the single column experiment setup used in experiments C1-C21

When conducting an experiment, the solution fed to the column was pumped through a degasser (Degassex DG-4400) and pumps 1 and 2 (Knauer P 4.1S). Pump 1 was used to pump loading solution, eluate, and desorption solutions, while pump 2 was used to pump water. The solutions continued to column which was heated by a water bath (Lauda C6 CS). After leaving the column, the sample solution circulated through a conductivity

measurement (Pharmacia Biotech), RI measurement, UV-vis measurement (Pharmacia Biotech UV-900) and a pH measurement (Consort C3210), and therefore online data was collected for some features of the column raffinate. After the measurements, the sample solution was either collected with a fraction collector or discarded as waste. The collected samples from the single column experiments were analyzed with Inductively Coupled Plasma Mass Spectrometer (ICP-MS) (Agilent 7850 ICP-MS), or Atomic Absorption Spectroscopy (AAS).

For the ICP-MS analytics, the samples were diluted with a 1 % HNO₃ and 1 % HCl matrix acid. The dilution of the samples was 10 000 times, which was done in two steps to 10 ml test tubes where dilution was 100 times.

For the AAS analytics, the samples were diluted with a 5% HNO₃ matrix acid. The dilution of the samples was 100 times.

6.1 LIWBL single column experiment

The first LIWBL single column experiment was done in order to determine the breakthrough times of lithium, cobalt and nickel, the metals targeted in the separation and copper, manganese, iron and aluminium, the metals they are to be separated from. This is necessary for designing the flowrates and switch times for the SMB runs, as there was not accurate enough data in previous literature. The experiment was also conducted with adjusting the multi metal solution pH at the operating temperature of 60 °C, since pH can affect the process greatly. The experiment was conducted by first feeding the multi metal solution into the column, eluding the rest of the metal solution out of the column with H₂O, and then desorbing it first with 1 M H₂SO₄ and then with 0.4 M K₂-oxalate. The column was regenerated with 1 M H₂SO₄ and rinsed with water after the experiment.

All of the different steps of this experiment were designed to deliberately long, so that it could be known for sure when all the metals broke through in the loading stage and when they were all eluted in the desorption stages. The parameters of the experiment are presented in Table VI.

Table VI Parameters of single column experiment C1

Temperature, C	60
Multi metal solution pH, -	1.8
Multi metal solution volume, BV	8.0
Elution volume, BV	6.0
Desorption 1 (H ₂ SO ₄) volume, BV	3.0
Desorption 2 (K ₂ -oxalate) volume, BV	4.0
Regeneration (H ₂ SO ₄) volume, BV	2.0
Multi metal solution flowrate, BV/h	2.0
Elution flowrate, BV/h	6.0
Desorption 1 (H ₂ SO ₄) flowrate, BV/h	2.0
Desorption 2 (K ₂ -oxalate) flowrate, BV/h	2.0
Regeneration (H ₂ SO ₄) flowrate, BV/h	2.0
Multi metal solution flow direction, -	bottom to top
Elution flow direction, -	bottom to top
Desorption 1 (H ₂ SO ₄) flow direction, -	top to bottom
Desorption 2 (K ₂ -oxalate) flow direction, -	top to bottom
Regeneration (H ₂ SO ₄) flow direction, -	top to bottom

6.1.1 LIWBL single column experiment results

All of the samples collected from this experiment were analyzed with ICP-MS.

The breakthrough curves of all metals are presented in Figure 7. The desired metals, lithium, cobalt and nickel broke through first, lithium and nickel at 0.8 BV and cobalt later at 1 BV. From 0.8 BV to 2 BV no other metals broke through in the process. This was the window to extract the desired product from the system, raffinate, when it was not contaminated with any other metals.

The first metals that broke through after the desired ones were manganese and copper at 2 BV, and aluminium at 3 BV. Iron was also present in the multi metal solution, but it did not break through within the 8 BV of multi metal solution feed.

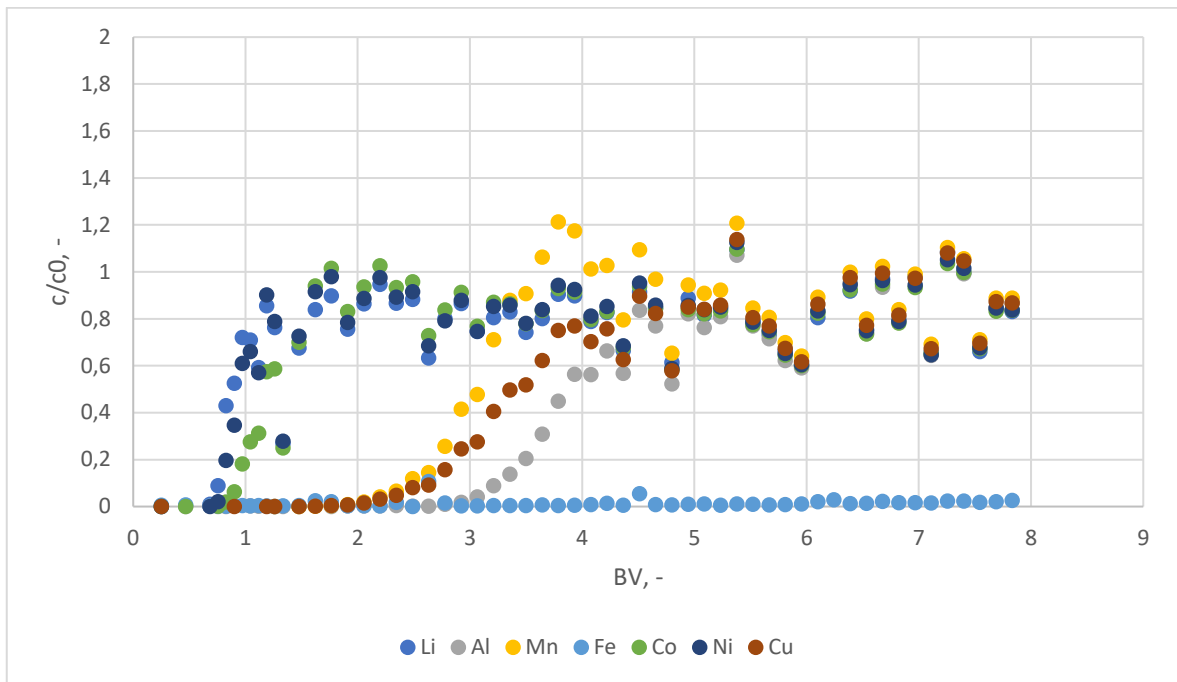


Figure 7 C1 metal breakthrough curves from aminomethylphosphonic acid functional Lewatit TP260 resin. Flowrate 2 BV/h and flow direction bottom to top. All of the tests done in one using a multi metal solution. T=60°C.

The elution curve for all the metals is presented in Figure 8. As can be seen from the graph, a lot of cobalt, nickel and lithium were lost in this step of the process because it was not included in the raffinate product. Naturally, a lot of the target metals were lost in this step since after the loading the column was still full of the multi metal solution, which the elution flushed out. After this step all of the metals in solution form were flushed from the column, and the remaining metals in the column were all adsorbed into the resin bed.

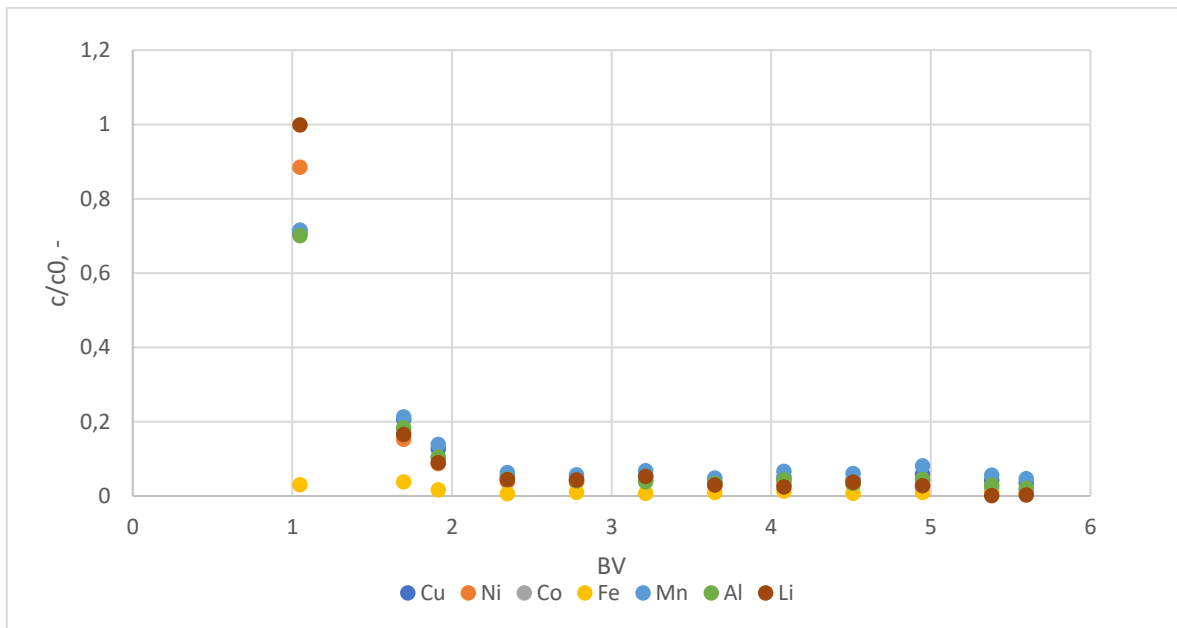


Figure 8 C1 elution graph from aminomethylphosphonic acid functional Lewatit TP260 resin. $T = 60^{\circ}\text{C}$. Flow rate 6 BV/h and flow direction bottom to top. Purified water used as eluent.

The desorption curve of the metals from desorption 1 is presented in Figure 9. The H_2SO_4 used in this step desorbs the manganese and copper, as can be seen from the Figure. The manganese and copper are fully desorbed from the column at about 1.5 BV. This step also desorbs some aluminium, but most of it is desorbed in desorption 2. The two-step desorption is necessary for this process because the H_2SO_4 is unable to desorb the iron and aluminium fully from the column. This step of the process produces extract 1, which contains the separated metals of copper and manganese. As can be seen from the graph, the extract 1 contains some aluminium and cobalt, which makes it impure.

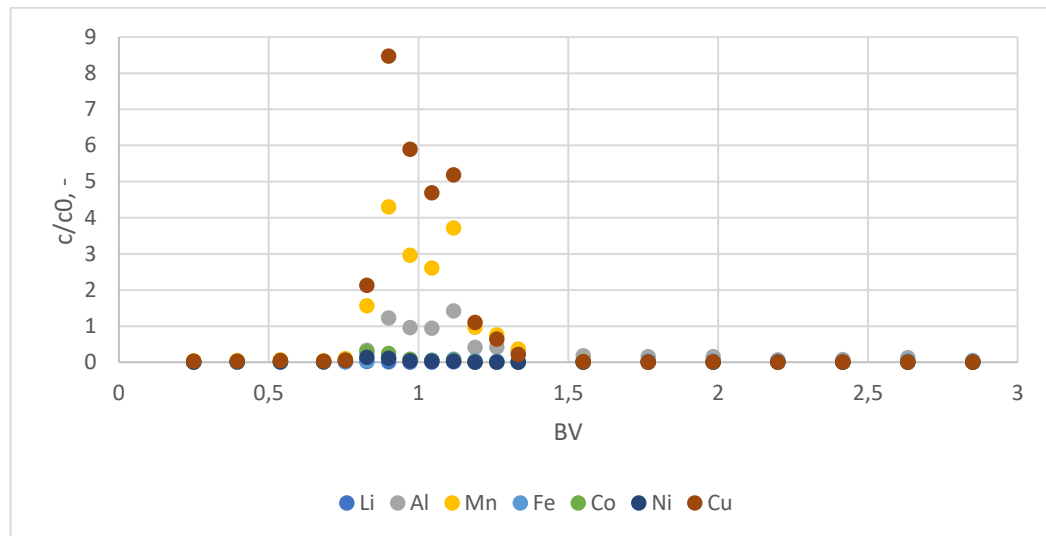


Figure 9 C1 desorption 1 graph from aminomethylphosphonic acid functional Lewatit TP260 resin. $T = 60^{\circ}\text{C}$. Flowrate 2 BV/h and flow direction top to bottom. 1 M H_2SO_4 used as desorbent.

The desorption curve of the metals from desorption 2 is presented in Figure 10. The K_2 -oxalate used in this step desorbs the remaining iron and aluminium, as can be seen from the Figure. The aluminium is desorbed from the column after 3 BV and iron after 4 BV. This step of the process produces extract 2, which contains the separated metals of iron and aluminium.

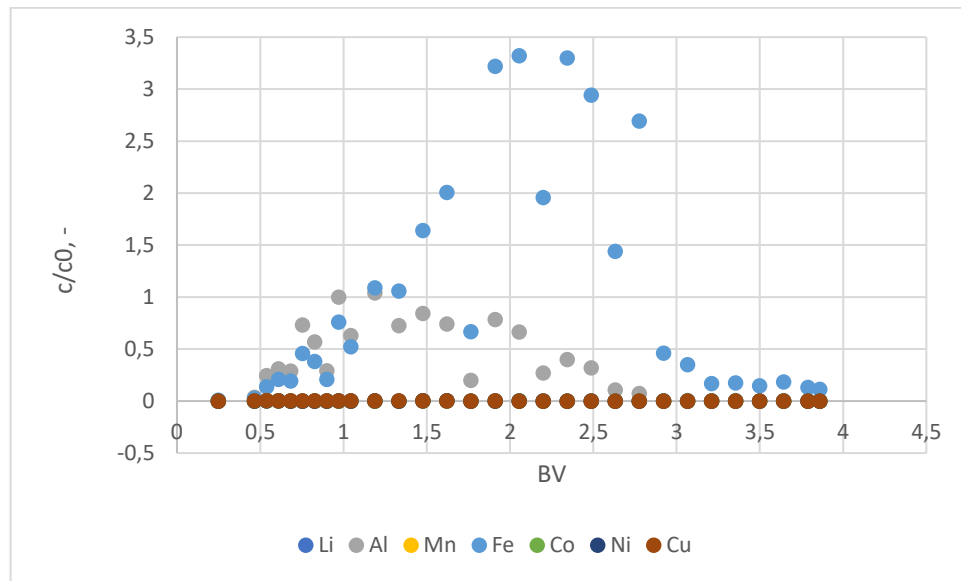


Figure 10 C1 desorption 2 graph from aminomethylphosphonic acid functional Lewatit TP260 resin. T = 60°C. Flowrate 2 BV/h and flow direction top to bottom. 0.4 M K-oxalate used as desorbent.

6.1.2 Recoveries of metals in LIWBL single column experiment

The target metals to separate to the raffinate in this process were lithium, cobalt and nickel. In an ideal process, their recovery to the raffinate would be 100 %, and no metals would be lost to elution, desorption 1 or desorption 2. The recoveries of the target metals in different parts of the process are presented in Table VII.

Table VII Recoveries of target metals in raffinate, elution, desorption1 and desorption 2 in single column experiment C1

	Raffinate, %	Elution, %	Desorption 1, %	Desorption 2, %
Cobalt	75.23	14.96	9.69	0.09
Lithium	82.31	13.11	4.46	0.09
Nickel	84.43	14.24	1.07	0.19

Out of the target metals 24.65 % of cobalt, 17.66 % of lithium and 15.5 % of nickel are lost to elution, desorption 1 and desorption 2. The remaining lithium and nickel are mainly recovered in elution, but especially cobalt is not eluted with the H₂O elution, and almost 10 % of it is lost to desorption 1. In the SMB, it would be possible to recycle the elution to the raffinate, and therefore recover most of the lithium and nickel, but even that would result in a large loss of cobalt.

6.2 Fe desorption experiments

In addition to single-column experiments with multi metal solution, experiments were also performed with solution containing only Fe in order to determine the time for the iron to fully desorb from the resin. The concentration of the Fe-solution was 741 mg/L, which is the same concentration that Fe has in the multi metal solution. These experiments were performed with 0.2 M Na₂-oxalate and 0.4 M K₂-oxalate and different volumes of Fe-solution feed. The lengths of Fe-solution feed and the oxalate used in the experiments are presented in Table VIII.

Table VIII Fe desorption experiments and their parameters

Experiment	Volume of Fe-solution, BV	Oxalate used
C5	0.5	Na ₂ -oxalate
C6	1.0	Na ₂ -oxalate
C7	1.5	Na ₂ -oxalate
C8	2.5	Na ₂ -oxalate
C9	2.5	K ₂ -oxalate
C10	4.5	Na ₂ -oxalate
C11	6.0	Na ₂ -oxalate
C15	0.5	K ₂ -oxalate
C16	1.0	K ₂ -oxalate
C17	1.5	K ₂ -oxalate
C18	4.5	K ₂ -oxalate
C19	6.0	K ₂ -oxalate

The volume of the Fe-solution ranged from 0.5 BV to 6.0 BV. The flowrate of the Fe-solution, the volume of oxalate solution and its flowrate were kept constant to determine the effect of the increase in the Fe-solution volume. The rest of the parameters of the Fe-solution experiments are presented in Table IX.

Table IX Fe desorption experiments parameters

Temperature, C	60
Fe-solution pH, -	1.8
Oxalate volume, BV	4.0
Oxalate flowrate, BV/h	6.0
Fe-solution flowrate, BV/h	6.0
Fe-solution flow direction, -	bottom to top
Oxalate flow direction, -	top to bottom

The Fe-solution experiments were performed by feeding the Fe-solution into the column, then feeding the oxalate to desorb the iron from the resin, and finally regenerating the resin with 1 M H₂SO₄ and flushing the column with water. In these experiments, only the desorption step was sampled and analyzed using AAS.

6.2.1 Fe desorption experiments results

Experiments C5-C8 and C10-C11 were performed with 0.2 M Na₂-oxalate, and they are presented in Figure 11.

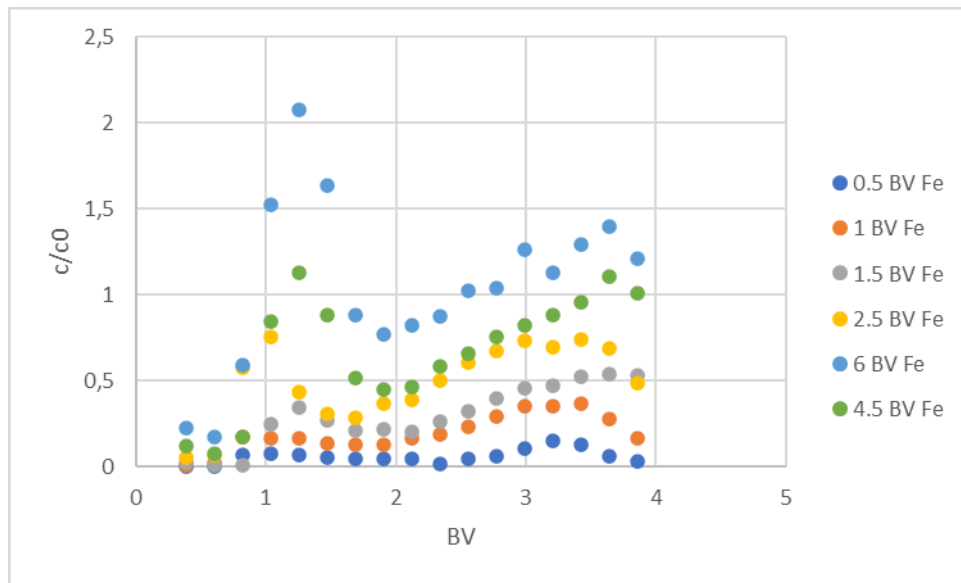


Figure 11 Results of experiments C5-C8 and C10-C11. Desorption of Fe from aminomethylphosphonic acid functional Lewatit TP260 resin. $T = 60^{\circ}\text{C}$. Flowrate of oxalate 6 BV/h and flow direction top to bottom. Oxalate used 0.2 M $\text{Na}_2\text{-oxalate}$. Flowrate of Fe-solution 6 BV/h and flow direction bottom to top.

As can be seen from Figure 11, the $\text{Na}_2\text{-oxalate}$ is not capable of desorbing the iron fully out of the resin with the oxalate volume of 4 BV. Experiments C9 and C15-C19 were performed using 0.4 M $\text{K}_2\text{-oxalate}$, and their graphs are presented in Figure 12.

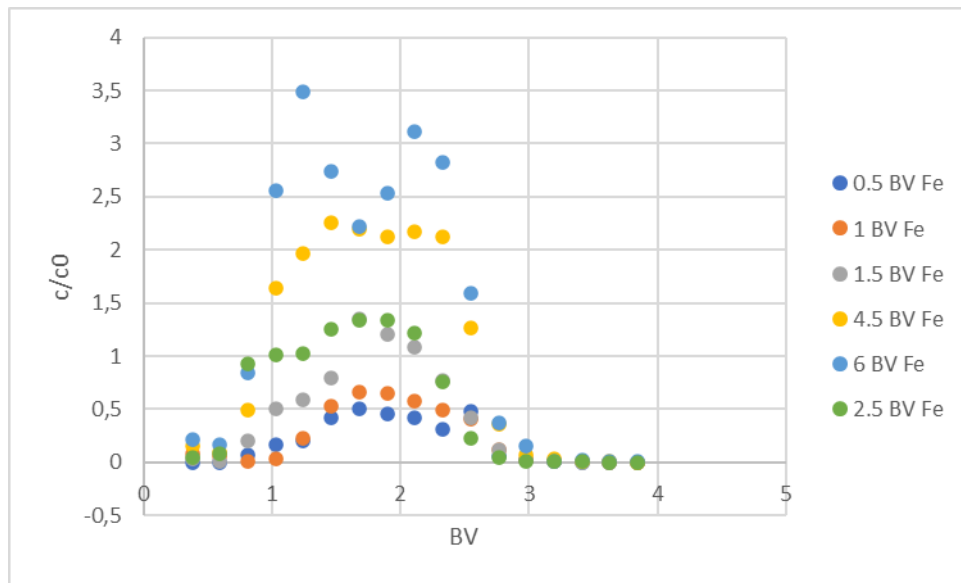


Figure 12 Results of experiments C9 and C15-C19. Desorption of Fe from aminomethylphosphonic acid functional Lewatit TP260 resin. $T = 60^{\circ}\text{C}$. Flowrate of oxalate 6 BV/h and flow direction top to bottom. Oxalate used 0.4 M K-oxalate. Flowrate of Fe-solution 6 BV/h and flow direction bottom to top.

As can be seen from Figure 12, the K_2 -oxalate desorbs the iron from the system much more effectively. Even though the different volumes of the Fe-solution feed affect the desorption, it can be seen that with 4 BV of K_2 -oxalate all iron leaves the system, even when the Fe-solution feed is the highest, 6 BV.

It also can be noticed from Figures 11 and 12 that with the desorptions of Na_2 -oxalate and the high volume desorptions of K_2 -oxalate, the peak of the iron leaving the column splits in to two. This is most likely related to the ratio of iron and oxalate in the system. The first peak, which is high, could be caused by low oxalate concentration and long second peak because of oxalate exhausted in the system. The concentration of Na_2 -oxalate in these experiments was only 0.2 M which is half of the 0.4 M of the K_2 -oxalate used. The concentration of Na_2 -oxalate cannot be higher since its highest solubility at room temperature is about 0.27 M (ChemBK 2022).

From these experiments it can be noticed that Na_2 -oxalate can not act as a substitute of K_2 -oxalate in the system. Even with the highest volume of iron fed into the column, the K_2 -oxalate is able desorb it with a volume of 4 BV.

6.3 Washing 1 M H₂SO₄ with raffinate

Due to the limited amount of motor valves available, the washing step in between the regeneration of the resin and loading may need to be eliminated for the system to work. If this step was taken out, it would be necessary to wash away the 1 M H₂SO₄ from the resin regeneration with the raffinate from the previous zone. In order to test if this would work, a washing experiment was conducted. The parameters of the experiment are presented in Table X.

Table X Parameters of single column experiment C2

Temperature, C	60
H ₂ SO ₄ concentration, M	2.0
K ₂ -oxalate concentration, M	0.4
H ₂ SO ₄ feed, BV	1.0
H ₂ SO ₄ flowrate, BV/h	6.0
K ₂ -oxalate feed, BV	1.0
K ₂ -oxalate flowrate, BV/h	6.0
Na ₂ SO ₄ concentration, M	0.85
Na ₂ SO ₄ feed, BV	4.0
Na ₂ SO ₄ flowrate, BV/h	6.0

Using the single column experiment setup, 1 BV of 0.4 M K₂-oxalate was fed into the column to mimic desorption and following that, 1 BV of 1 M H₂SO₄ was fed to the column to mimic regeneration. After these inlets, 4.0 BV of 0.85 M Na₂SO₄ was fed to the column to mimic the front of the metal solution, and to see how well it washes away the 1 M H₂SO₄ left from the loading. The conductivity of the Na₂SO₄ feeding step was analyzed to determine the results.

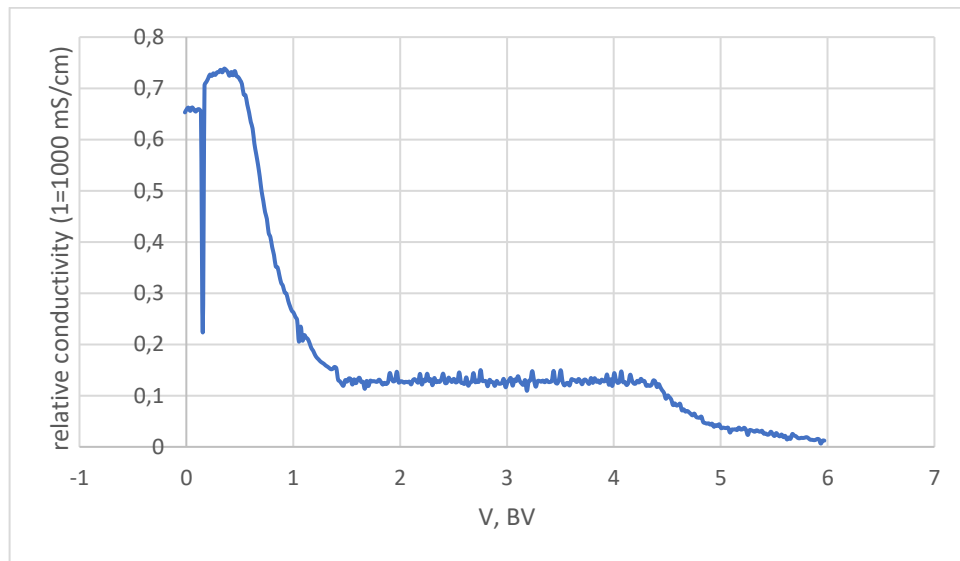


Figure 13 Conductivity graph of 0.7 M Na₂SO₄ feed after regeneration of resin in experiment C2. Conductivity reaching 0 when all regenerate is washed out. 1.0 M H₂SO₄ used as regenerate.

As can be seen from the conductivity graph in Figure 13, the conductivity after the regeneration step is high, but feeding the Na₂SO₄ solution to the levels it off to 0.1. After the Na₂SO₄ solution was fed to the column for 4.0 BV, the column was rinsed with purified water, which lowers the conductivity to 0. From this experiment, it can be concluded that washing away the 1 M H₂SO₄ with the raffinate in the SMB will work, and an additional washing step can be skipped. This does not cause an issue in the outlets, as mixing the raffinate with the 1 M H₂SO₄ will only result in more acidic raffinate.

6.4 Single column experiment with SMB switch times using TP260 resin

Before the SMB experiment was conducted, a single column experiment with the same settings was done to mimic one cycle of the SMB. This experiment was done with a concentrated multi metal solution and a 50 % diluted multi metal solution to mimic the mixing of the eluent and raffinate that would happen in the SMB.

The eluent after the multi metal solution was changed to 1.8 pH H₂SO₄ in order to elude the cobalt that was lost to desorption 1 in C1 to the raffinate. To mimic the SMB, all of the steps of the experiment were adjusted to the same amount of time, which was chosen to be

25 minutes. This adjustment was done with modifying the flowrates. In the SMB the switch times need to be quick, i.e. 25 minutes, so the flowrates can be high. In experiments C13 and C14 it was also tested if the process can function with higher flowrates.

The experiment was done twice, C13 with the concentrated multi metal solution and C14 with the 50 % diluted metal solution. The diluted multi metal solution used in experiment C14 mimics the SMB with the elution recycling the best. The parameters for experiments C13 and C14 are presented in Table XI.

Table XI Parameters of single column experiments C13 and C14

Multi metal solution pH, -	1.8
Temperature, C	60
Multi metal solution volume, BV	2.5
Elution volume, BV	1.5
Desorption 1 (H ₂ SO ₄) volume, BV	2.5
Desorption 2 (K ₂ -oxalate) volume, BV	2.5
Regeneration (H ₂ SO ₄) volume, BV	1.0
Multi metal solution flowrate, BV/h	6.0
Elution flowrate, BV/h	3.6
Desorption 1 (H ₂ SO ₄) flowrate, BV/h	6.0
Desorption 2 (K ₂ -oxalate) flowrate, BV/h	6.0
Regeneration (H ₂ SO ₄) flowrate, BV/h	2.4
Multi metal solution flow direction, -	bottom to top
Elution flow direction, -	bottom to top
Desorption 1 (H ₂ SO ₄) flow direction, -	top to bottom
Desorption 2 (K ₂ -oxalate) flow direction, -	top to bottom
Regeneration (H ₂ SO ₄) flow direction, -	top to bottom

6.4.1 Single column experiment with SMB switch times using TP260 resin experiment results

The C13 loading phase graph is presented in Figure 14. As can be seen from the Figure, the undesired metals of copper and manganese start to break through only at about 1.5 BV, which is much earlier than observed in the earlier experiments. It can also be seen that aluminium starts to break through at 1.7 BV which is also much earlier than in previous experiments. This is most likely due to the increase of flowrates.

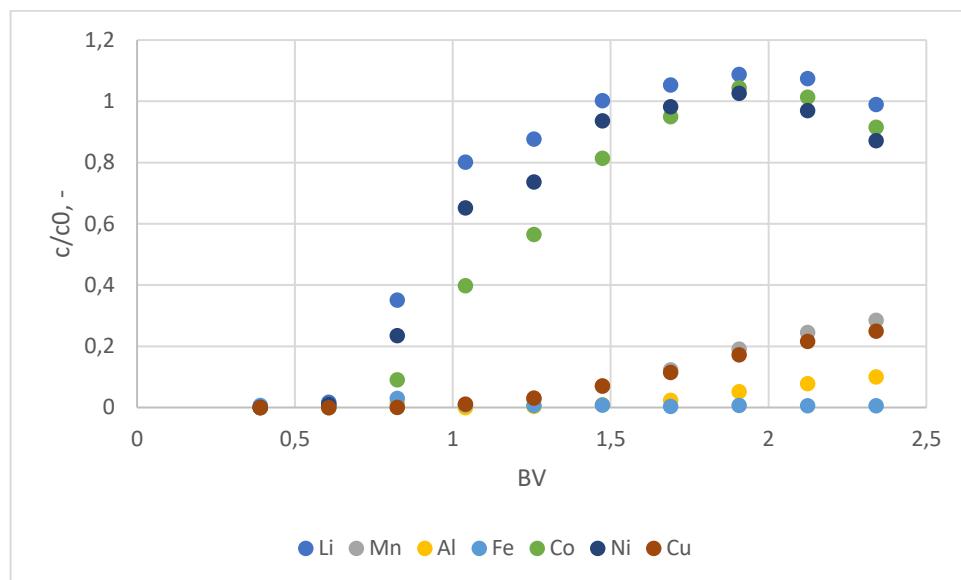


Figure 14 C13 Loading ICP graph from aminomethylphosphonic acid functional Lewatit TP260 resin. $T = 60^{\circ}\text{C}$. Flowrate 6 BV/h and flow direction bottom to top.

The C13 desorption 1 graph is presented in Figure 15. Desorption 1 was 2.5 BV in length, but as can be seen from the Figure copper and manganese are barely fully desorbed from the column and cobalt is lost to desorption 1.

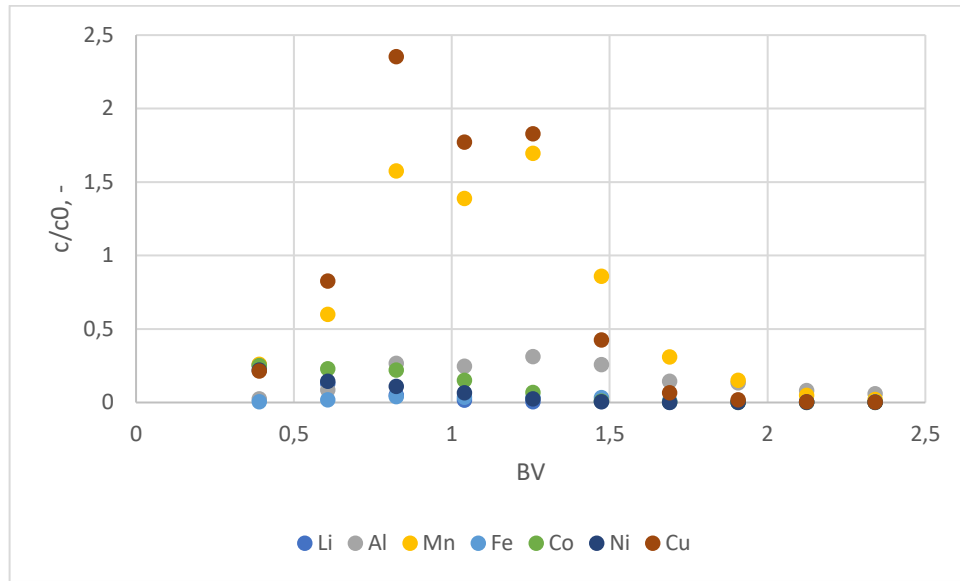


Figure 15 C13 Desorption 1 ICP graph from aminomethylphosphonic acid functional Lewatit TP260 resin. T = 60°C. Flowrate 6 BV/h and flow direction top to bottom. 1 M H₂SO₄ used as desorbent.

The ICP graph from desorption 2 is presented in Figure 16. As can be seen from the Figure, the iron and aluminium do not fully desorb from the column with the 2.5 BV desorption.

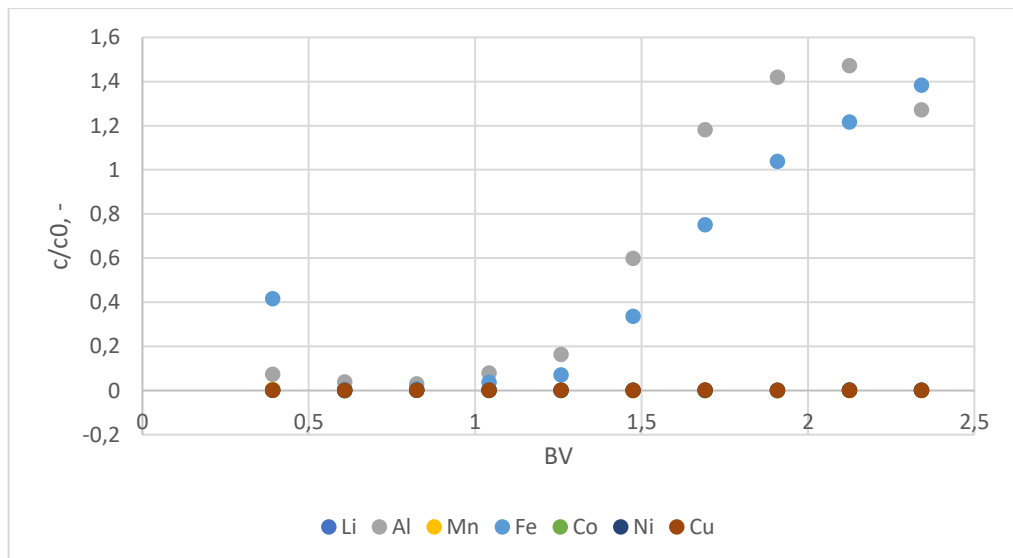


Figure 16 C13 Desorption 2 ICP graph from aminomethylphosphonic acid functional Lewatit TP260 resin. T = 60°C. Flowrate 6 BV/h and flow direction top to bottom. 0.4 M K-oxalate used as desorbent.

The ICP graph of regeneration is presented in Figure 17. As can be seen from the Figure, iron and aluminium still desorb from the column during the regeneration, and the iron still has a full peak during the regeneration.

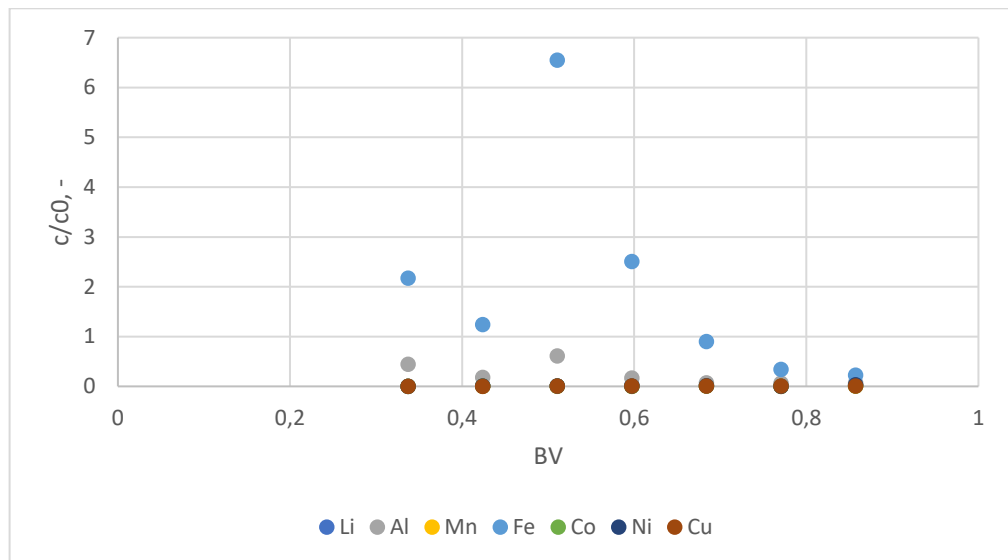


Figure 17 C13 Regeneration graph from aminomethylphosphonic acid functional Lewatit TP260 resin. T = 60°C. Flowrate 2.4 BV/h and flow direction bottom to top. 1 M H₂SO₄ used as regenerate.

6.4.2 Single column experiment with SMB switch times using TP260 resin and 50 % diluted metal solution experiment results

All of the samples collected from this experiment were analyzed with ICP-MS.

The C14 loading phase graph is presented in Figure 18. As can be seen from the Figure, the undesired metals of copper and manganese start to break through only at about 1.5 BV, later than observed in C13. Also opposed to C13, aluminium does not break through in this experiment.

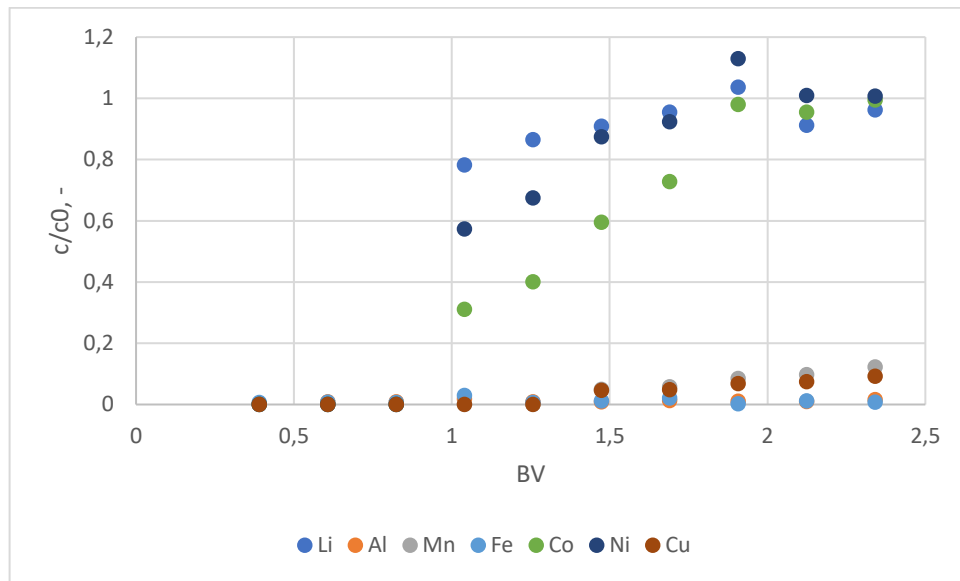


Figure 18 C14 Loading ICP graph from aminomethylphosphonic acid functional Lewatit TP260 resin. T = 60°C. Flowrate 6 BV/h and flow direction bottom to top. 50 % diluted multi metal solution used.

The C14 desorption 1 graph is presented in Figure 19. Desorption 1 was 2.5 BV in length, but as can be seen from the Figure copper and manganese are barely fully desorbed from the column and cobalt is lost to desorption 1 more than in C13.

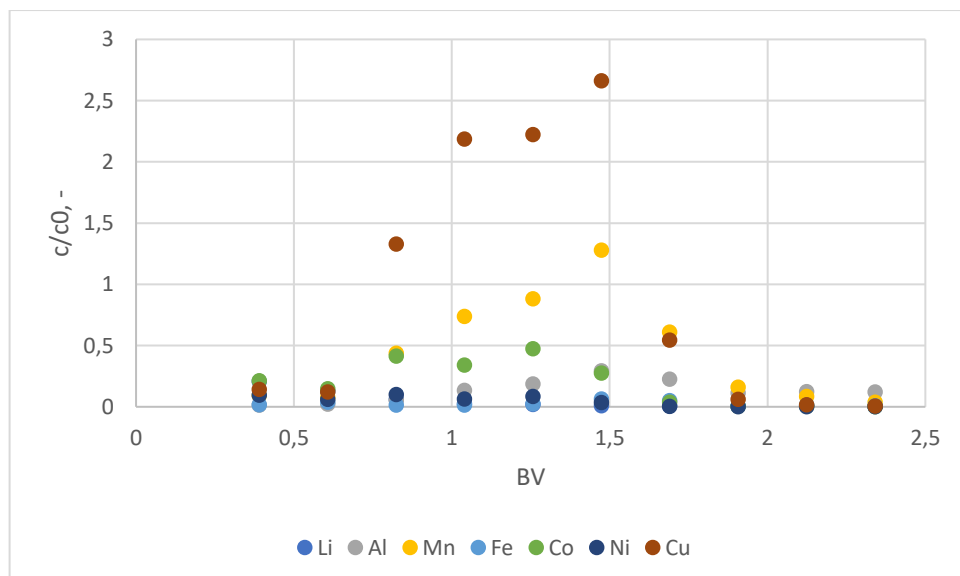


Figure 19 C14 Desorption 1 ICP graph from aminomethylphosphonic acid functional Lewatit TP260 resin. T = 60°C. Flowrate 6 BV/h and flow direction top to bottom. 1 M H₂SO₄ used as desorbent.

The ICP graph of the desorption 2 is presented in Figure 20. As can be seen from the graph, the iron and aluminium do not fully desorb from the column during the 2.5 BV desorption 2.

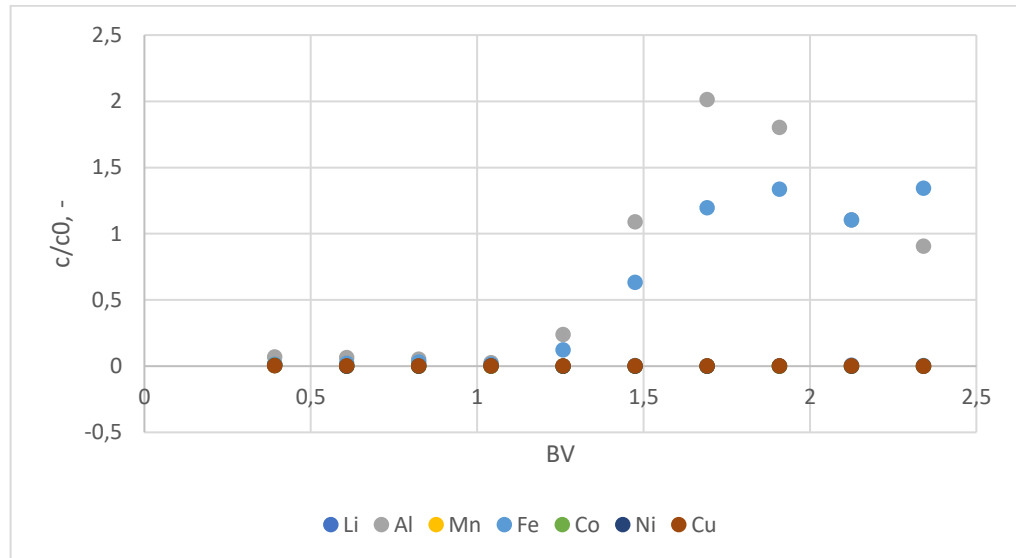


Figure 20 C14 Desorption 2 ICP graph from aminomethylphosphonic acid functional Lewatit TP260 resin. T = 60°C. Flowrate 6 BV/h and flow direction top to bottom. 0.4 M K-oxalate used as desorbent.

The ICP graph of regeneration is presented in Figure 21. As can be seen from the Figure, iron and aluminium still desorb from the column during the regeneration.

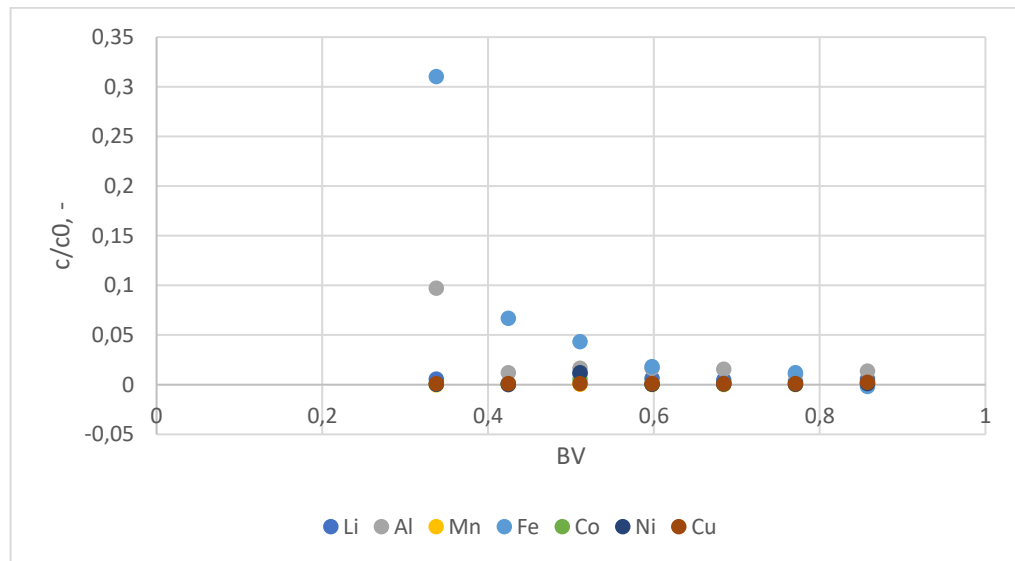


Figure 21 C14 Regeneration ICP graph from aminomethylphosphonic acid functional Lewatit TP260 resin. T = 60°C. Flowrate 2.4 BV/h and flow direction bottom to top. 1 M H₂SO₄ used as regenerate.

The early breakthrough of the undesired metals in the loading phase creates an issue, since the window to collect product with the target metals becomes very narrow, therefore decreasing the productivity of the process. The desorption steps would need to be lengthened as well, creating additional costs to the system.

6.5 Single column experiment with SMB switch times using MDS TP260 resin

Due to the issues in experiments C13 and C14 with the mass transfer and the early breakthrough of undesired metals when using higher flowrates, a new type of resin was tested to see if the issues could be solved using it. The MDS TP260 resin is similar to TP260, but it has a much smaller bead size. This smaller bead size creates a shorter diffusion path in the pores, which results in faster kinetics. This could allow the higher flowrates to work within the process.

Experiments C20 and C21 were conducted similarly to C13 and C14 but with a different resin. The desorption 1, desorption 2 and regeneration steps were extended to fully see the desorption of metals, to make sure that all of the metals were desorbed from the column.

The experiment was done twice, C20 with the concentrated multi metal solution and C21 with the 50 % diluted metal solution. The parameters for experiments C20 and C21 are presented in Table XII.

Table XII Parameters of single column experiments C20 and C21

Multi metal solution pH, -	1.8
Temperature, C	60
Multi metal solution volume, BV	2.5
Elution volume, BV	1.5
Desorption 1 (H ₂ SO ₄) volume, BV	4.0
Desorption 2 (K ₂ -oxalate) volume, BV	4.0
Regeneration (H ₂ SO ₄) volume, BV	2.5
Multi metal solution flowrate, BV/h	6.0
Elution flowrate, BV/h	3.6
Desorption 1 (H ₂ SO ₄) flowrate, BV/h	6.0
Desorption 2 (K ₂ -oxalate) flowrate, BV/h	6.0
Regeneration (H ₂ SO ₄) flowrate, BV/h	6.0
Multi metal solution flow direction, -	bottom to top
Elution flow direction, -	bottom to top
Desorption 1 (H ₂ SO ₄) flow direction, -	top to bottom
Desorption 2 (K ₂ -oxalate) flow direction, -	top to bottom
Regeneration (H ₂ SO ₄) flow direction, -	top to bottom

6.5.1 Single column experiment with SMB switch times using MDS TP260 resin experiment results

All of the samples from this experiment were analyzed with ICP-MS.

The C20 loading phase graph is presented in Figure 22. As can be seen from the Figure, the undesired metal of copper starts to break through only at about 2.25 BV, which is much later than with the experiment C13, which was executed with resin with larger particle size.

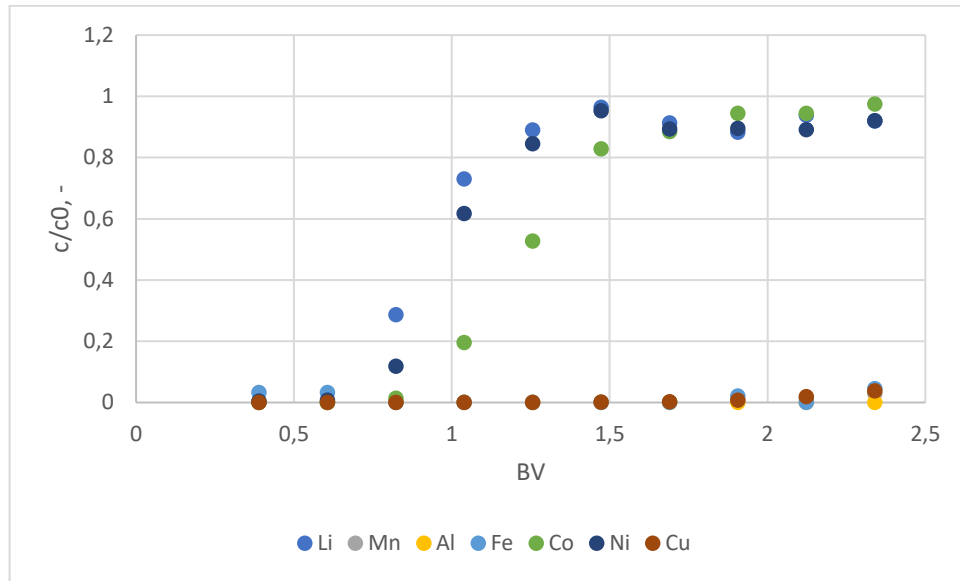


Figure 22 C20 Loading ICP graph from aminomethylphosphonic acid functional Lewatit MDS TP260 resin. $T = 60^{\circ}\text{C}$. Flowrate 6 BV/h and flow direction bottom to top.

The C20 desorption 1 graph is presented in Figure 23. Desorption 1 was lengthened to 4 BV, and as it can be seen from the Figure, manganese and copper are fully desorbed from the column by 2 BV.

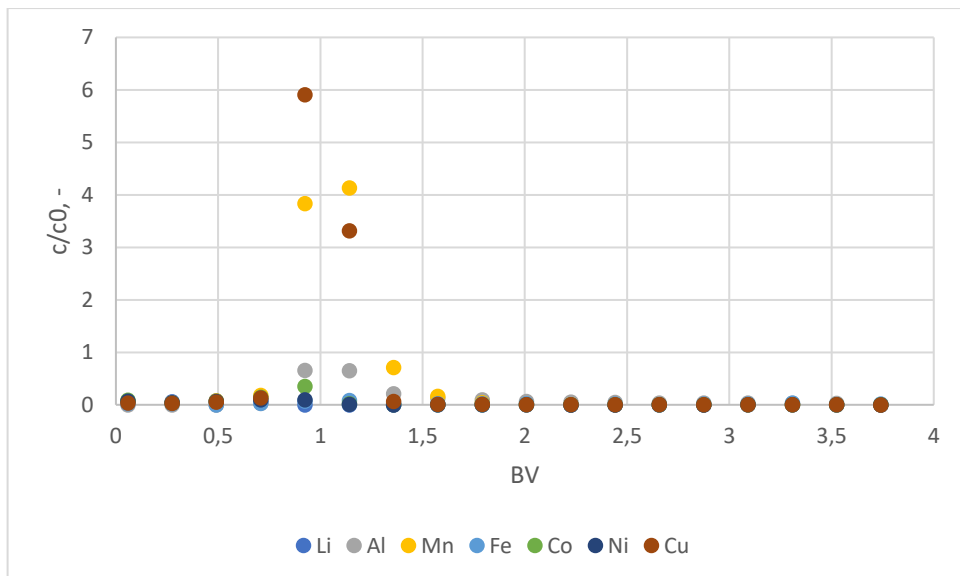


Figure 23 C20 Desorption 1 ICP graph from aminomethylphosphonic acid functional Lewatit MDS TP260 resin. $T = 60^{\circ}\text{C}$. Flowrate 6 BV/h and flow direction top to bottom. 1 M H_2SO_4 used as desorbent.

The desorption 2 graph is presented in Figure 24. The iron and aluminium are fully desorbed from the column at about 3.5 BV, which is a great improvement from experiments C13 and C14.

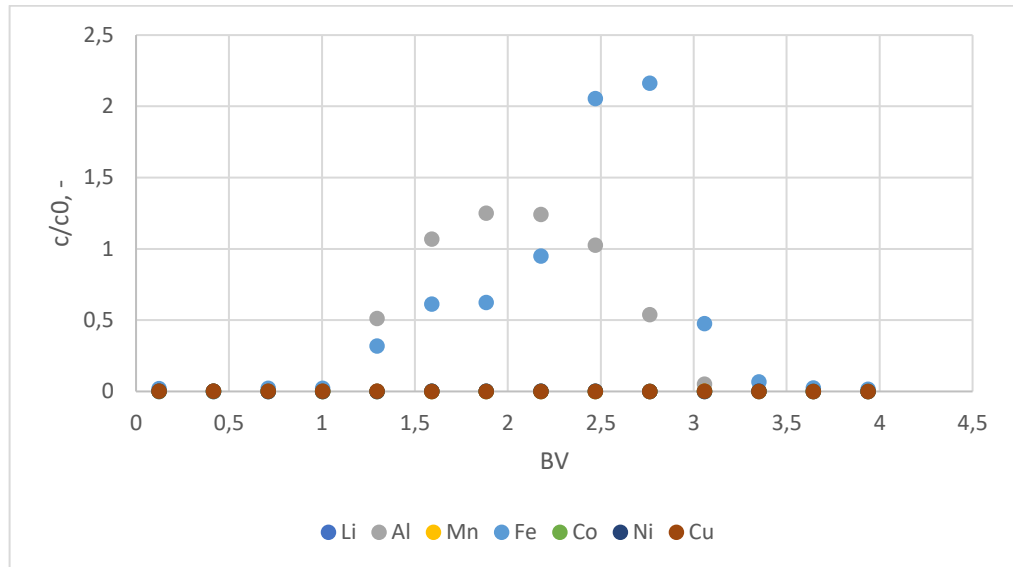


Figure 24 C20 Desorption 2 ICP graph from aminomethylphosphonic acid functional Lewatit MDS TP260 resin. T = 60°C. Flowrate 6 BV/h and flow direction top to bottom. 0.4 M K-oxalate used as desorbent.

The regeneration graph is presented in Figure 25. All of the metals are fully desorbed from the column during desorption 1 and desorption 2, which is an improvement from previous experiments.

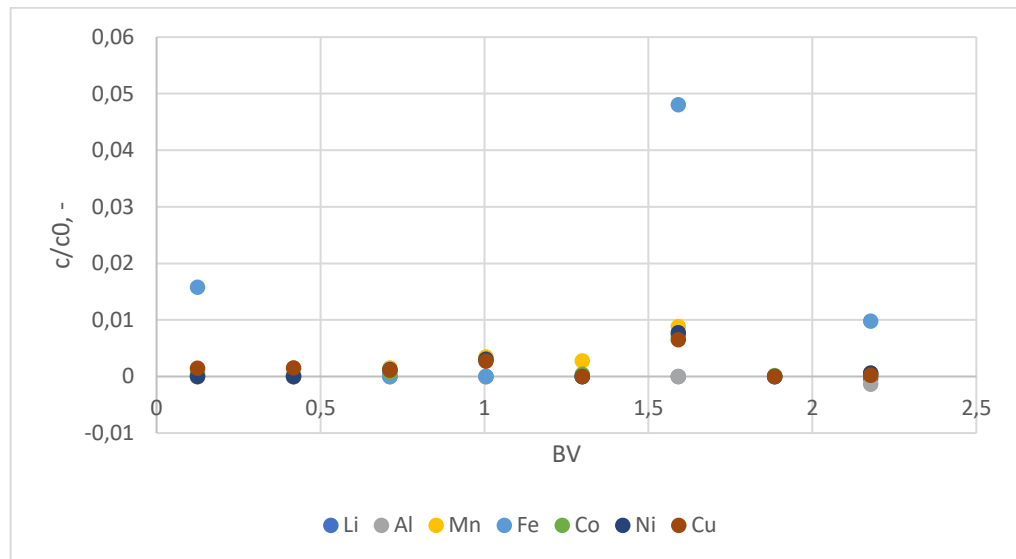


Figure 25 C20 Regeneration ICP graph from aminomethylphosphonic acid functional Lewatit MDS TP260 resin. T = 60°C. Flowrate 6 BV/h and flow direction bottom to top. 1 M H₂SO₄ used as regenerate.

6.5.2 Single column experiment with SMB switch times using MDS TP260 resin and 50 % diluted metal solution experiment results

All of the samples from this experiment were analyzed with ICP-MS.

The C21 loading phase graph is presented in Figure 26. As can be seen from the Figure, the undesired metals don't break through at all by 2.5 BV. This experiment is performed with the diluted multi metal solution and mimics the SMB with the elution recycling the best. We can also see the most separation between the target metals in this experiment, with lithium breaking through at about 0.6 BV, nickel at 0.75 BV and cobalt only at 1 BV. This shows the possibility to develop a process to recover all of the target metals separately.

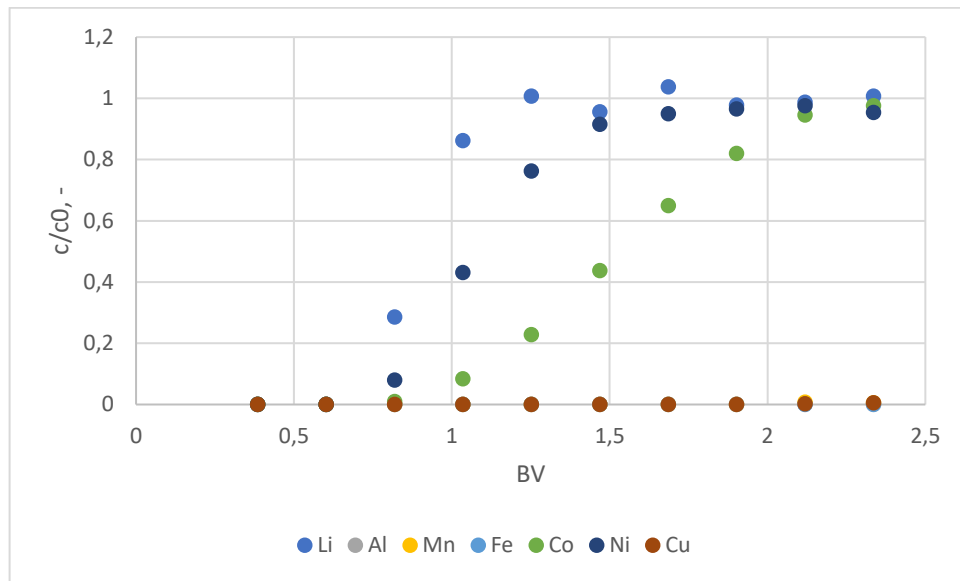


Figure 26 C21 Loading ICP graph from aminomethylphosphonic acid functional Lewatit MDS TP260 resin. T = 60°C. Flowrate 6 BV/h. Flow direction bottom to top.

The C21 desorption 1 graph is presented in Figure 27. Desorption 1 was lengthened to 4 BV, and as it can be seen from the Figure, manganese and copper are fully desorbed from the column by 2.5 BV. In this Figure, it can also be seen that some of the cobalt is not eluted in the elution step since it is desorbed in desorption 1 step, and therefore its total recovery is lowered.

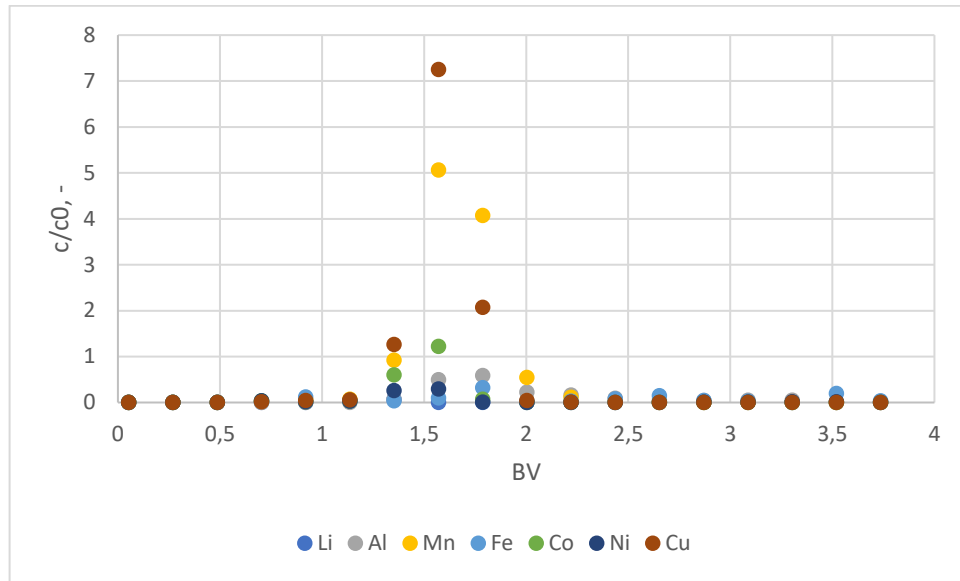


Figure 27 C21 Desorption 1 ICP graph from aminomethylphosphonic acid functional Lewatit MDS TP260 resin. $T = 60^{\circ}\text{C}$. Flowrate 6 BV/h and flow direction top to bottom. 1 M H_2SO_4 used as desorbent.

The desorption 2 graph is presented in Figure 28. The iron and aluminium are fully desorbed from the column at about 3 BV, which is a great improvement from experiments C13 and C14.

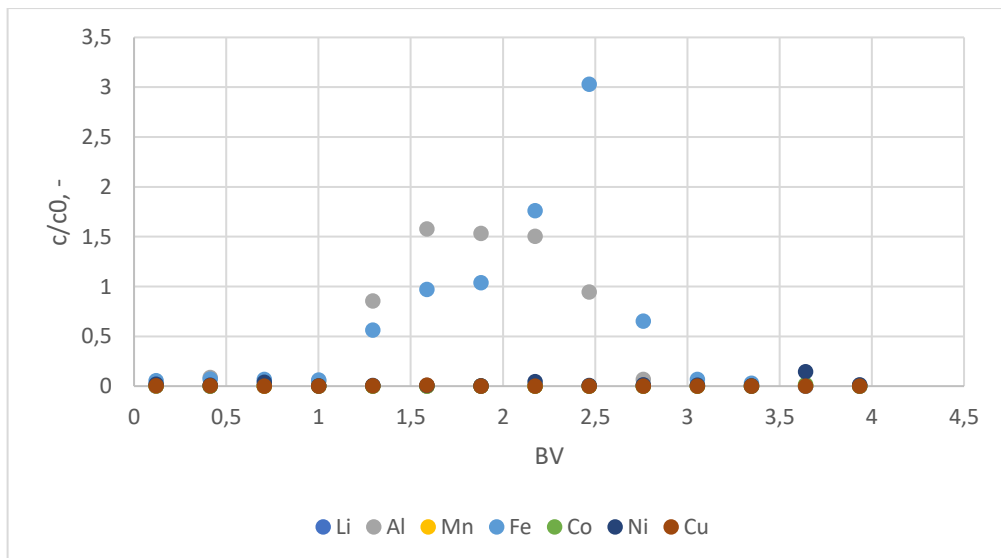


Figure 28 C21 Desorption 2 ICP graph from aminomethylphosphonic acid functional Lewatit MDS TP260 resin. $T = 60^{\circ}\text{C}$. Flowrate 6 BV/h and flow direction top to bottom. 0.4 M K-oxalate used as desorbent.

The regeneration graph is presented in Figure 29. All of the metals are fully desorbed from the column during desorption 1 and desorption 2, which is an improvement from previous experiments, and the process works as expected. None of the impurities break trough within the loading step and all of the impurities are desorbed from the column during desorption 1 and desorption 2.

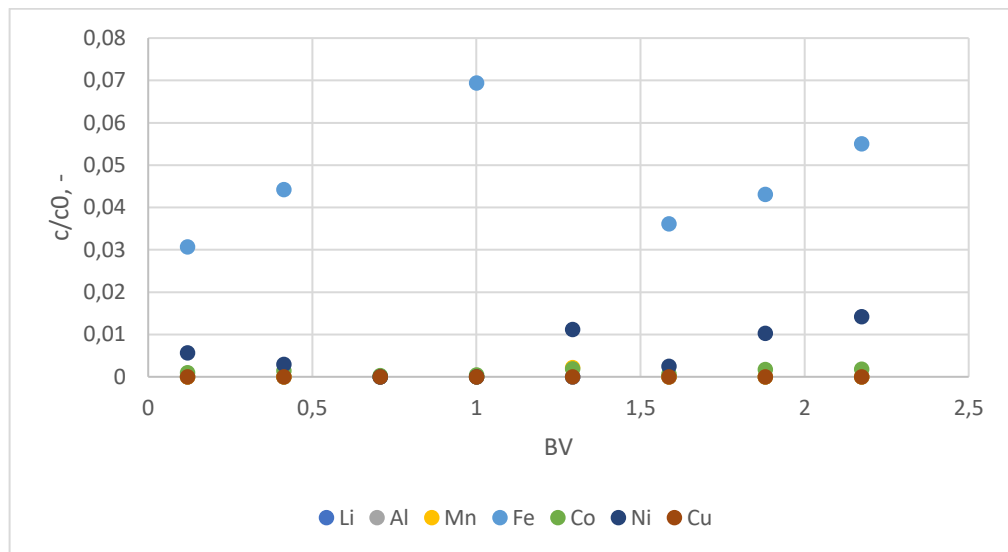


Figure 29 C21 Regeneration ICP graph from aminomethylphosphonic acid functional Lewatit MDS TP260 resin. T = 60°C. Flowrate 6 BV/h and flow direction bottom to top. 1 M H₂SO₄ used as regenerate.

6.5.3 Single column experiment with SMB switch times using MDS TP260 resin metal recoveries and losses

As could be seen from Figures 23 and 27, cobalt is lost to desorption 1 in both experiments C20 and C21. The amount of cobalt lost is presented in Table XIII. In experiments C20 and C21 it is assumed that the elution step would be recycled to the raffinate, as it would be in the SMB system.

Table XIII Cobalt loss in single column experiments C20 and C21

Experiment	Cobalt loss, %
C20	5.92 %
C21	17.9 %

Cobalt loss is the main problem in the process after the improvements. It is especially notable in C21, where 17.9 % of cobalt is not recovered in the product. C21 was conducted using the 50 % diluted multi metal solution, which mimics the SMB process when the elution is recycled to the raffinate, diluting the multi metal solution. The cobalt loss could be caused by the fact that the more diluted metal solution contains less of the impurities, and because of that, some of the cobalt gets adsorbed to the resin, and is only released during desorption 1. Possible solutions for this issue could be to feed more multi metal solution to the column, which can be explored during the SMB experiments.

6.6 Conclusions of the single column experiments

One of the main objects for the single column experiments was to determine the breakthrough times of the metals. This was experimented on in C1. When using the resin with the larger bead size, Lewatit TP260, the breakthrough times for the metals were determined as 0.8 BV for nickel and lithium, 1 BV for cobalt, 2 BV for manganese and copper and 3 BV for aluminium. Iron did not break through during the 8 BV of the experiment.

It was also determined from experiment C1 that during desorption 1 manganese and copper were desorbed after feeding 1.5 BV of 1 M H₂SO₄. During desorption 2 aluminium was fully desorbed after 3 BV of 0.4 M K-oxalate but iron was not fully desorbed after the 4 BV, which was the extent of the step.

From this experiment, it was concluded that the desired product can be collected until manganese and copper break through, which in this process is until 2 BV of the multi metal solution have been fed to the column. Manganese and copper can be desorbed using 1.5 BV of 1 M H₂SO₄, but 4 BV of 0.4 M K-oxalate was not able to fully desorb all the aluminium and iron.

Since the desorption of iron never reached fully zero during experiment C1, the desorption of iron was experimented on further during experiments C5-C11 and C15-C19. In the experiments, a 741 mg/L iron solution was fed to the column for 0.5, 1, 1.5, 2.5, 4.5 and 6 BV, and desorbed with 0.4 M K-oxalate or 0.2 M Na₂-oxalate for 4 BV.

From these experiments, it was concluded that the 0.2 M Na₂-oxalate was not able to fully desorb the iron in any of the experiments. The desorption of iron with 0.4 M K-oxalate was successful in all the experiments. It was concluded that 4 BV of 0.4 M K-oxalate is sufficient to desorb all the iron in the process.

Since there were a few limitations with the construction of the SMB, some of the steps from the single column experiments may needed to be combined or eliminated. One of the possible steps to exclude was the washing step after the regeneration. In experiment C4 it was experimented on if the multi metal solution used in the loading would be able to wash away the 1 M H₂SO₄ used in the regeneration.

From this experiment, it was concluded that the multi metal solution was able to wash away the 1 M H₂SO₄ used in the regeneration, the conductivity reaching neutral after the wash. The washing after regeneration step therefore can be eliminated from the process.

Since it was concluded from experiment C1 that a lot of the cobalt was lost to the elution and desorption of the process, it was determined that in the SMB system the elution and loading fractions should be combined. Combining them would result in a more diluted metal solution. This was experimented on during experiment C14, where the metal solution was 50 % diluted. During experiments C13 where 100 % metals solution was used and C14 where 50 % metal solution was used the flow rates of the different steps were also adjusted, as the steps need to be faster when in the SMB system. The time for each step in the SMB system was chosen as 25 minutes.

From these experiments, it was concluded that the higher flowrates of the solutions led to much earlier breakthroughs of the undesired metals, copper, and manganese breaking through at 1.25 BV at C13 and at 1.5 at C14, and aluminium breaking through at 1.7 at C13. This leaves the time to collect the raffinate to be significantly shorter and would make the process very inefficient.

Since it was concluded from experiments C13 and C14 that there were challenges with the mass transfer using Lewatit TP260 resin and the higher flowrates, it was experimented on if a resin with smaller bead size would solve the issue. This was experimented on during experiments C20 and C21, where experiments C13 and C14 were redone using Lewatit MDS TP260 resin. In these experiments, the desorption 1 and desorption 2 steps were also extended to be fully sure of the desorption of the impurities.

From these experiments, it was concluded that the resin with the smaller particle size was able to achieve the mass transfer using the higher flowrates. None of the undesired metals broke through within the 2,5 BV of loading in either C20 or C21. The main issue in the process after these single column experiments is the cobalt loss, especially in experiment C21 which is the experiment mimicking the elution recycling to the raffinate with the 50 % diluted multi metal solution, losing 17.9 % cobalt to desorption 1.

Running the single column process as it is developed here is time consuming and demands a lot of labor. Some of the issues with it like the recovery of cobalt can be improved upon and will be improved upon in the SMB system. Using the single column process, it is not possible to recycle the elution to the loading fraction while the process is running, but the fractions could be combined when collecting them. The process does work as a single column process, but its efficiency and yield can be significantly improved using the SMB system.

7 CONSTRUCTION OF THE SIMULATED MOVING BED SYSTEM

The final experiments of the Thesis were conducted in a simulated moving bed (SMB). The system was designed off of the results of the single column experiments and some limiting factors (i.e. the amount of motor valves available). The flow diagram of the SMB setup is presented in Figure 30.

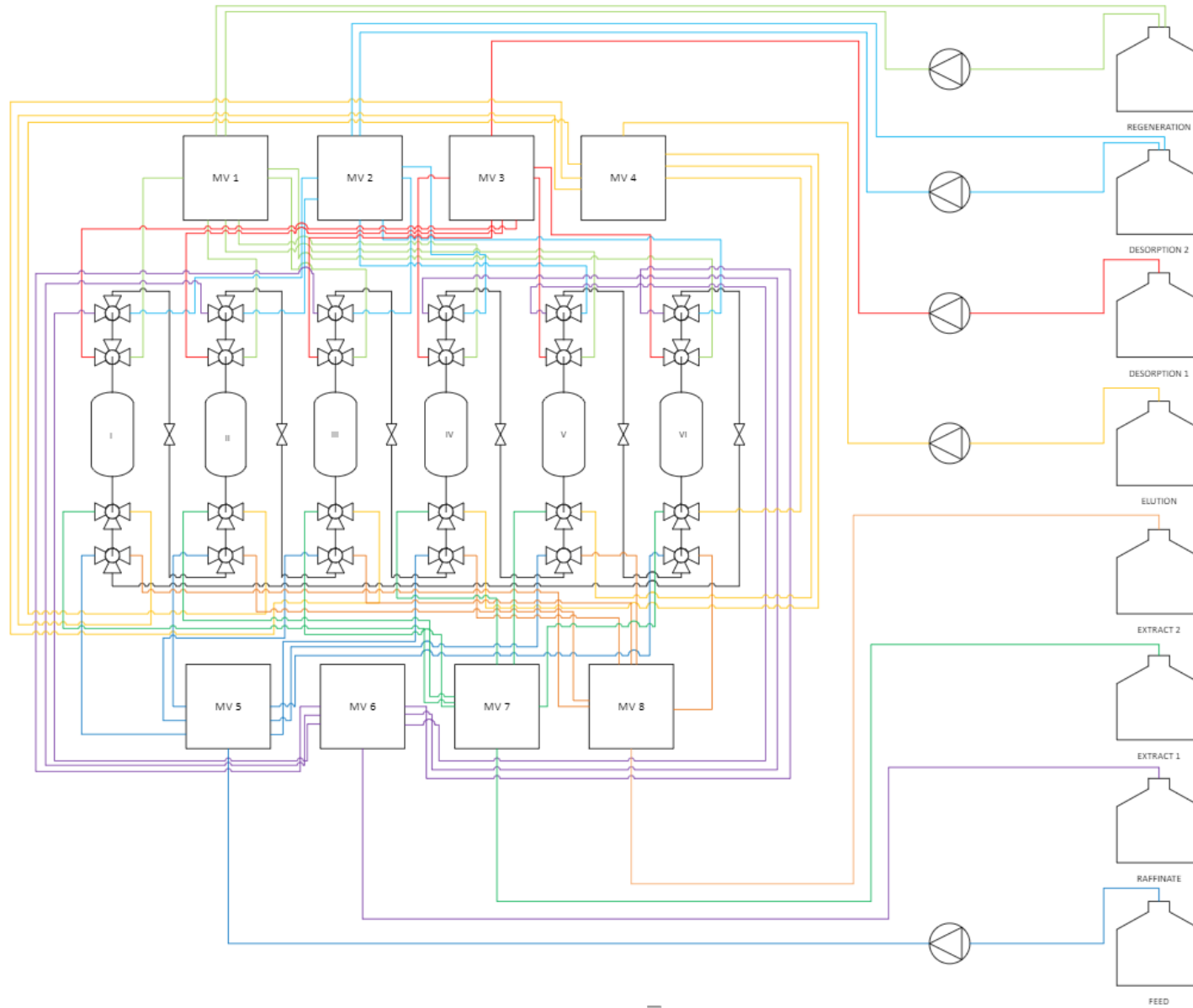


Figure 30 Flow diagram of the SMB setup

The SMB setup used eight motor valves, six columns packed with MDS TP260 resin, twenty-four t-valves, six solenoid valves, a heating bath (Lauda PROLINE RP 855), a pH meter (Consort C3060), two degasers (Desgassex DG-4400) and five pumps (Knauer P 4.1S).

When conducting the experiment, the solutions were pumped through two degassers to five different motor valves. From the motor valves, the solution traveled to the columns using twenty-four t-valves. In the first switch of the SMB, in the first configuration the multi metal feed solution was fed to column 4 and cycled through three columns using the solenoid valves in between them to exit the raffinate from column six. The elution solution was fed to column three, and in order to recover the cobalt, the elution solution was cycled to the multi metal feed solution flow with a solenoid valve between columns three and four. The desorption 1 solution was fed to column two and exited it through motor valve seven to extract 1. The desorption 2 and regeneration solutions were fed to column one and exited column one through motor valve eight to extract 2. When exiting the columns, the solutions were pumped through three motor valves to three different outlets through three pH meters: raffinate for the desired product of cobalt, nickel and lithium, extract 1 for the separated metals of copper and manganese and extract 2 for the separated metals of iron and aluminium.

Because of the limited amount of motor valves, the steps of desorption 2 and regeneration were combined in to one column. Because of this, the switches within the SMB were divided in to two parts; the regeneration solution and desorption 2 solution were pumped through motor valves 1 and 2. In the first part of the switch, desorption 2 solution was pumped to the column and regeneration solution recycled back to its bottle. In the second part, regeneration solution was pumped to the column and desorption 2 solution recycled back to the bottle. All the configurations of the other motor valves stayed the same during these two parts of the switch.

The switches were controlled through changing the motor valve ports. Each motor valve had 12 ports, and in the process six of them were connected to the columns and one to a waste container for cleaning and filling the lines without disturbing the process. Ports 1 through 6 were connected to their corresponding column and port 11 to a waste container. In motor valves 1 and 2 port 7 was connected to their solution bottle to form a recycling line. The configuration of the motor valve ports is presented in Table XIV.

The cycling of the elution and multi metal feed solution between several columns is controlled by solenoid valves in between the columns. The solenoid valves are open when the solution is cycled and closed when it is not. Each solenoid valve is situated after its corresponding column, i.e. solenoid valve 1 is situated between columns 1 and 2. The solenoid valves open and close in the same configuration as the motor valves. The configuration of the solenoid valves is presented in Table XV. In Table XV, O means that the solenoid valve is open, and X means that the solenoid valve is closed.

Table XIV Configuration of the motor valve ports in the SMB system

No. of motor valve		No. of switch											
		1	2	3	4	5	6	7	8	9	10	11	12
valve	1	1	7	2	7	3	7	4	7	5	7	6	7
	2	7	1	7	2	7	3	7	4	7	5	7	6
	3	2	2	3	3	4	4	5	5	6	6	1	1
	4	3	3	4	4	5	5	6	6	1	1	2	2
	5	4	4	5	5	6	6	1	1	2	2	3	3
	6	6	6	1	1	2	2	3	3	4	4	5	5
	7	2	2	3	3	4	4	5	5	6	6	1	1
	8	1	1	2	2	3	3	4	4	5	5	6	6

Table XV Configuration of solenoid valves in the SMB system (O=open, X=closed)

No. of solenoid valve		No. of switch											
		1	2	3	4	5	6	7	8	9	10	11	12
valve	1	X	X	X	X	O	O	O	O	O	O	X	X
	2	X	X	X	X	X	X	O	O	O	O	O	O
	3	O	O	X	X	X	X	X	X	O	O	O	O
	4	O	O	O	O	X	X	X	X	X	X	O	O
	5	O	O	O	O	O	O	X	X	X	X	X	X
	6	X	X	O	O	O	O	O	O	X	X	X	X

8 SIMULATED MOVING BED EXPERIMENTS

For the Thesis, three simulated moving bed experiments were conducted. The goal was to achieve an experiment that would result in the highest possible recovery and purity of the desired metals of lithium, nickel and cobalt. The SMB experiments and their aims are presented in Table XVI.

Table XVI Aims of the SMB experiments

Experiment	Aim
SMB1	SMB with design parameters based on the single column experiments
SMB2	Increase of multi metal solution feed from 1 BV in SMB 1 to 2 BV to increase cobalt, lithium, and nickel recovery
SMB3	Increase of multi metal solution feed to 2.5 BV to increase cobalt recovery

8.1 SMB 1

The design of SMB 1 (Table XVII), was based on the results received from the single column experiments of C20-21.

The duration of the experiment was chosen to be 24 switches, since that would achieve four full cycles for the process, and it was assumed that the process would be in steady state.

Table XVII Parameters of experiment SMB 1

Switch time, min	25 min
Temperature, C	60
Multi metal solution pH, -	1.8
Amount of switches completed	24
Multi metal solution feed, BV	1.0
Elution feed, BV	1.5
Desorption 1 feed, BV	2.5
Desorption 2 feed, BV	4.0
Regeneration feed, BV	1.5
Multi metal solution flowrate, BV/h	2.4
Elution flowrate, BV/h	3.6
Desorption 1 flowrate, BV/h	6.0
Desorption 2 flowrate, BV/h	13.2
Regeneration flowrate, BV/h	13.2
Duration of the experiment, h	10

All of the three outlets, raffinate, extract 1 and extract 2 were sampled as aggregate samples, meaning that one switch yielded one sample. After the experiment was over, the columns were treated with desorbent 1 and desorbent 2 to compile a solid phase axial profile to more accurately find out how the metals were present in each column after every phase of the process.

8.2.1 SMB 1 results

The results of the raffinate samples analyzed from switches 1-24 are presented in Figure 31. It can be seen that the cobalt content in the samples is much lower than the content of nickel and lithium, and its recovery therefore will be much lower.

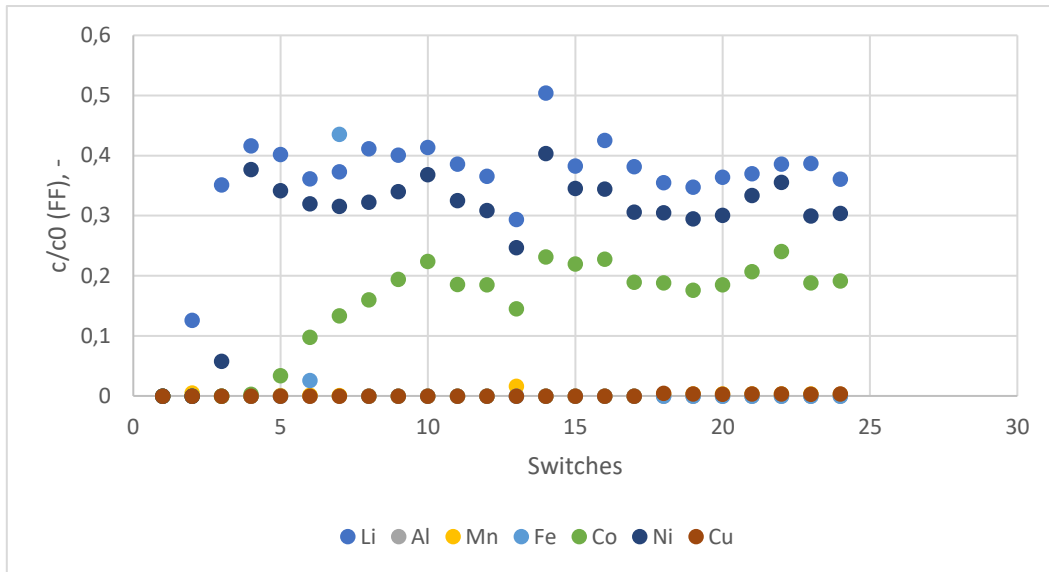


Figure 31 ICP analysis of switch 1-24 of raffinate in SMB 1 from aminomethylphosphonic acid functional Lewatit MDS TP260 resin. $T = 60^{\circ}\text{C}$. Flowrate of loading 2.4 BV/h and of elution 3.6 BV/h. Flow direction bottom to top. Eluent used 1.8 pH H_2SO_4 .

The results of the extract 1 samples analyzed from switches 1-24 are presented in Figure 32. It can be seen from the photo, that in addition to manganese and copper, the desired metals to be desorbed in this step, large amounts of cobalt, nickel and aluminium are also desorbed. The cobalt and nickel desorption at this step account for their lower recovery rate in the raffinate.

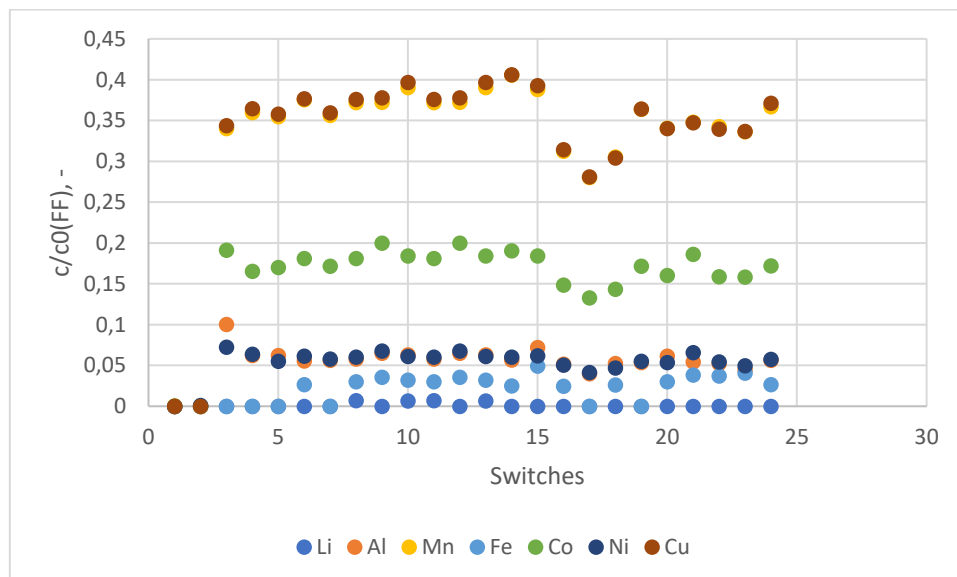


Figure 32 ICP analysis of switch 1-24 of extract 1 in SMB 1. Desorption from aminomethylphosphonic acid functional Lewatit MDS TP260 resin. $T = 60^{\circ}\text{C}$. Flowrate 6 BV/h. Flow direction top to bottom. Desorbent used 1 M H_2SO_4 .

The results of the extract 2 samples analyzed from switches 1-24 are presented in Figure 33. In this step, desorption 2 and regeneration are combined. It can be seen from the Figure that only iron and aluminium are desorbed at this step, which means that all the other metals were desorbed successfully at previous steps.

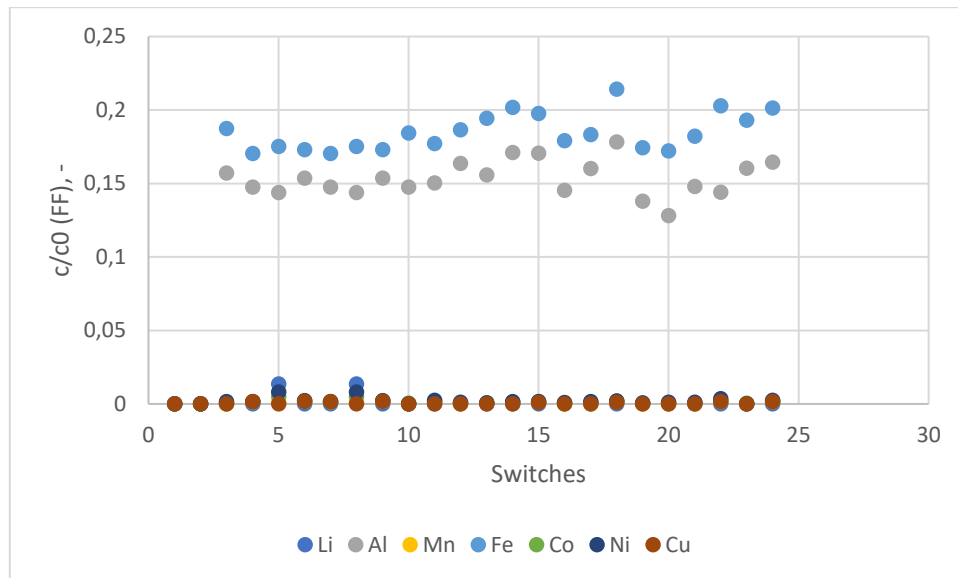


Figure 33 ICP analysis of switch 1-24 of extract 2 in SMB 1. Desorption from aminomethylphosphonic acid functional Lewatit MDS TP260 resin. $T = 60^{\circ}\text{C}$. Flowrate of Desorption 2 and regeneration 13.2 BV/h. Flow direction top to bottom. Desorbent used 0.4 M $\text{K}_2\text{-oxalate}$, regenerate used 1 M H_2SO_4 .

The solid phase axial profile of SMB 1 is presented in Figure 34. This Figure is after switch 24 is completed, and switch 25 should start next with a new cycle. There are no metals in column 6, which has just been regenerated, and only iron and aluminium in column 1, which has just been through desorption 1. As expected, column 3 contains all the metals, since multi metal solution has been fed into it, and columns 4 and 5 contain the target metals, lithium, nickel and cobalt. Column 2 has just been eluted, and it should not contain any of the target metals, but as can be seen, the elution was not successful and in addition to cobalt, also nickel is left in the column.

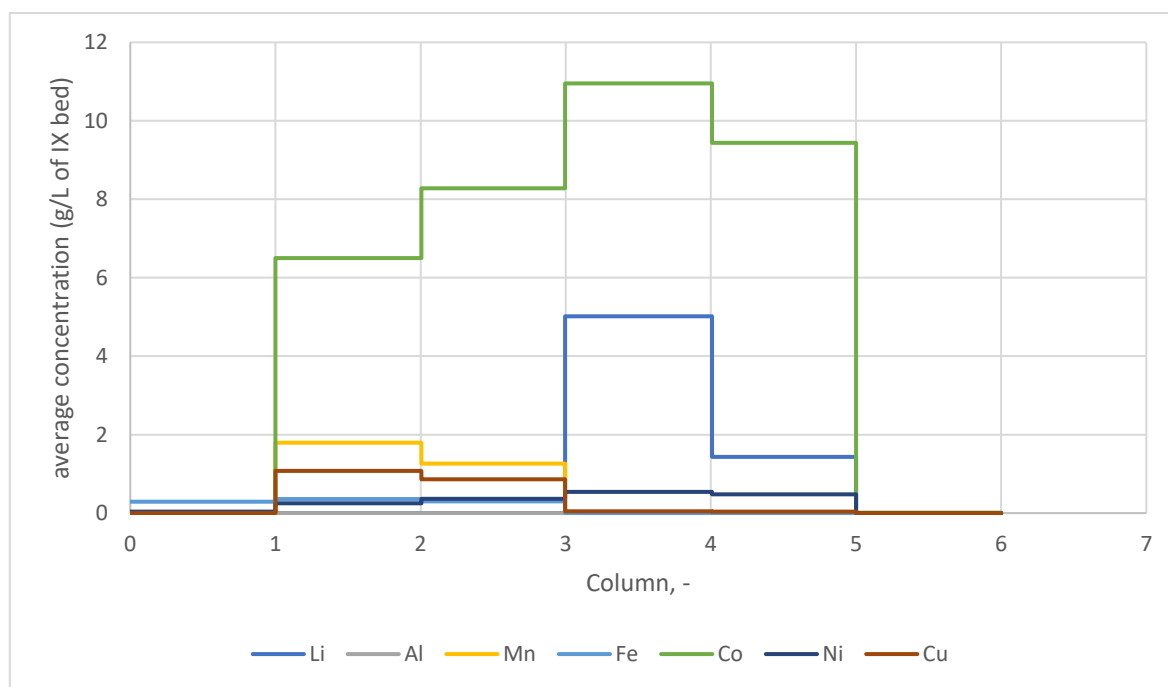


Figure 34 Solid phase axial profile after switch 24 in SMB 1

The recoveries of the metals in different steps are presented in Table XVIII. As can be seen, up to 43% of cobalt is lost to extract 1 and about 15 % of nickel. The purities of the outlets are presented in Table XIX. Raffinate The purity of raffinate is 99.5 %, so no undesired metals are in it. The impurity of extract 1 is due to the large amount of cobalt, nickel and aluminium in it.

As can be seen from Tables XVIII and XIX, the issue with the outcome of this run is the low recovery of the desired metals, especially cobalt and nickel. The purities of the outlets are good. The purity of extract 1 is low, but it will increase when nickel and cobalt are recovered in the raffinate, not in extract 1.

Table XVIII Single-metal recoveries in raffinate, extract1 and extract 2 in experiment SMB 1

	Li	Al	Mn	Fe	Co	Ni	Cu
Raffinate	93.11	0.41	0.54	6.07	49.08	81.64	0.29
recovery, %							
Extract 1	0.31	14.83	89.18	5.93	43.38	14.62	89.78
recovery, %							
Extract 2	0.34	38.18	0.19	46.95	0.37	0.53	0.14
recovery, %							

Table XIX Raffinate, extract 1 and extract 2 purities in experiment SMB 1

Raffinate (Co, Li, Ni), %	99.46
Extract 1 (Cu, Mn) , %	69.42
Extract 2 (Fe, Al), %	96.57

8.2 SMB 2

The second SMB experiment, SMB 2, was based on the results received from SMB 2. All the parameters were based on those experiments and are presented in Table XX.

The duration of the experiment was chosen to be 20 switches since the process in SMB 1 was assumed to be in steady state before the 20 switches. Due to the cobalt and nickel losses in SMB 1, the multi metal solution feed was doubled to 2 BV to hopefully achieve a successful elution of cobalt for higher cobalt recovery in the raffinate. The increase in the feed of the multi metal solution naturally increased the amount of impurities fed to the system. The increased number of impurities could fill up the adsorbing capacity of the resin, and so result in less cobalt adsorbing to the resin. The increase of the multi metal solution also increases the productivity of the process.

Table XX Parameters of experiment SMB 2

Switch time, min	25 min
Temperature, C	60
Multi metal solution pH, -	1.8
Amount of switches completed	20
Multi metal solution feed, BV	2.0
Elution feed, BV	1.5
Desorption 1 feed, BV	2.5
Desorption 2 feed, BV	4.0
Regeneration feed, BV	1.5
Multi metal solution flowrate, BV/h	4.8
Elution flowrate, BV/h	3.6
Desorption 1 flowrate, BV/h	6.0
Desorption 2 flowrate, BV/h	13.4
Regeneration flowrate, BV/h	13.4
Duration of the experiment, h	8.33

All of the three outlets, raffinate, extract 1 and extract 2 were sampled as aggregate samples, meaning that one switch yielded one sample. After the experiment was over, the columns were treated with desorbent 1 and desorbent 2 to compile a solid and liquid phase axial profile to more accurately find out how the metals were present in each column after every phase of the process.

8.2.1 SMB 2 results

The results of the raffinate samples analyzed from switches 1-20 are presented in Figure 35. It can be seen that the cobalt content in the samples is much higher than in SMB 1, and it can be assumed that its recovery will be much higher. The higher cobalt content is caused by the decrease of the amount of cobalt adsorbed by the resin. When impurities are adsorbed to the resin from the multi metal solution instead of the cobalt, it allows the cobalt continue towards the outlet without being adsorbed to the resin along the way, resulting in a higher content in the raffinate.

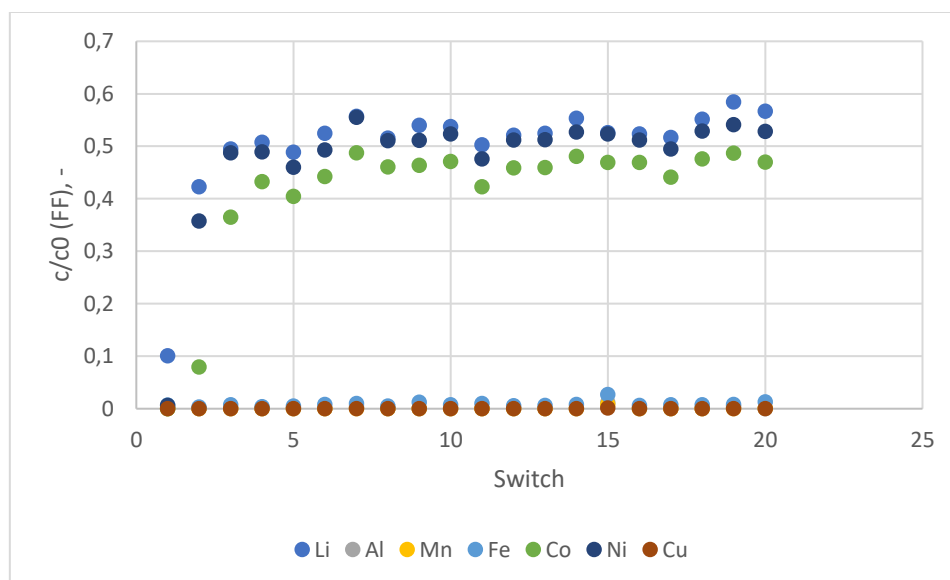


Figure 35 ICP analysis of switch 1-20 of raffinate in SMB 2 from aminomethylphosphonic acid functional Lewatit MDS TP260 resin. $T = 60^{\circ}\text{C}$. Loading flowrate 4.8 BV/h, elution flowrate 3.6 BV/h. Flow direction top to bottom. Eluent used 1.8 pH H_2SO_4 .

The results of the extract 1 samples analyzed from switches 1-20 are presented in Figure 36. It can be seen from the Figure, that in addition to manganese and copper, the desired metals to be desorbed in this step, some cobalt and aluminium are also desorbed. The cobalt desorption at this step account for its lower recovery rate in the raffinate, but much less than in SMB 1.

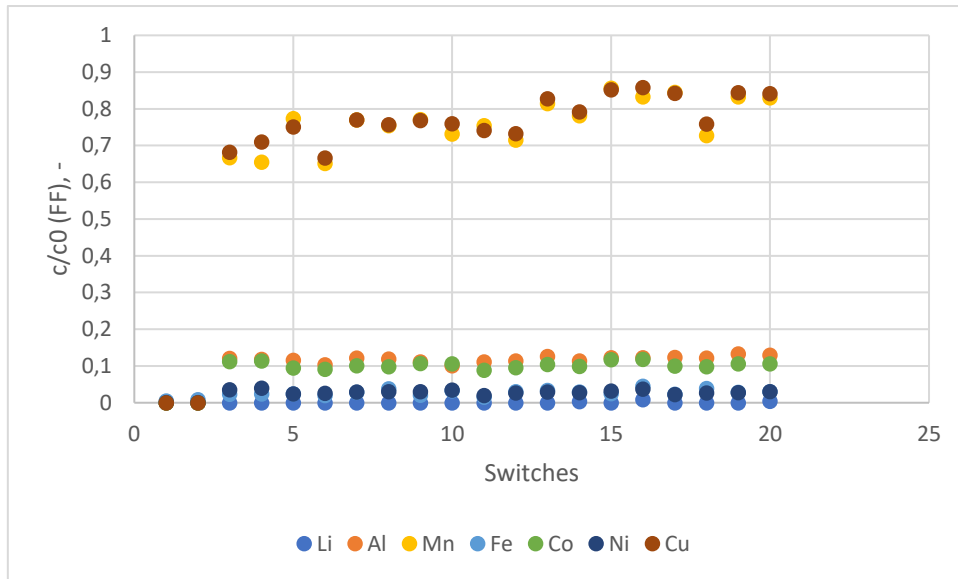


Figure 36 ICP analysis of switch 1-20 of extract 1 in SMB 2. Desorption from aminomethylphosphonic acid functional Lewatit MDS TP260 resin. $T = 60^{\circ}\text{C}$. Flowrate 6 BV/h. Flow direction top to bottom. Desorbent used 1 M H_2SO_4 .

The results of the extract 2 samples analyzed from switches 1-20 are presented in Figure 37. In this step, desorption 2 and regeneration are combined. It can be seen from the Figure that only iron and aluminium are desorbed at this step, which means that all the other metals were desorbed successfully at previous steps.

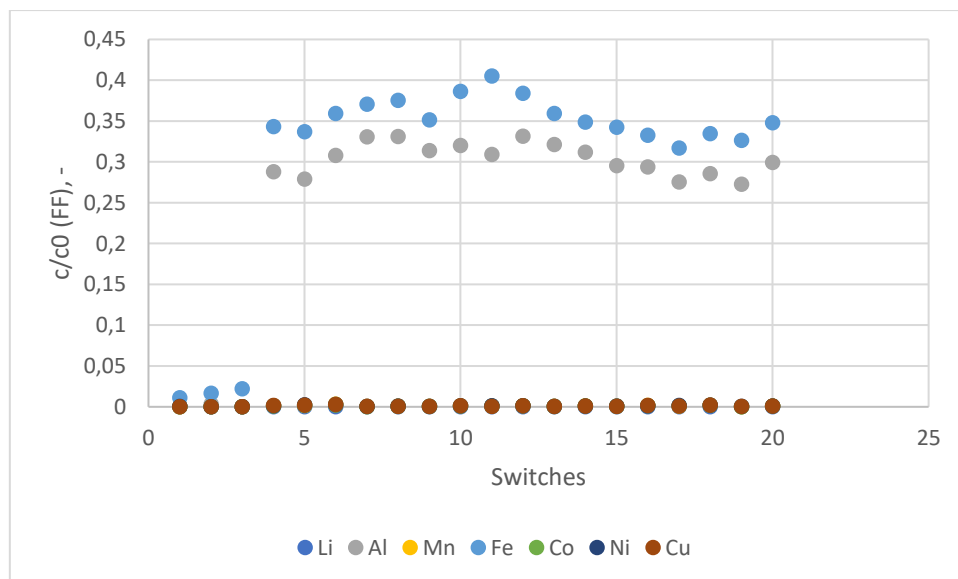


Figure 37 ICP analysis of switch 1-20 of extract 2 in SMB 2. Desorption from aminomethylphosphonic acid functional Lewatit MDS TP260 resin. $T = 60^{\circ}\text{C}$.

Flowrate of Desorption 2 and regeneration 13.2 BV/h. Flow direction top to bottom.
Desorbent used 0.4 M K_2 -oxalate, regenerate used 1 M H_2SO_4 .

The solid and liquid phase axial profile of SMB 2 is presented in Figure 38. The axial profile is after switch 20 is completed, which would be followed by switch 21. Column 2 contains no metals, which has just been regenerated. Column 3 only contains iron and aluminium, which has just been in desorption 1. Column 5 contains all metals, since multi metal solution has been fed into it. Columns 6 and 1 contain the target metals, lithium, cobalt and nickel. Column 4 still contains some cobalt despite having just been eluted, so the elution step was still not fully successful.

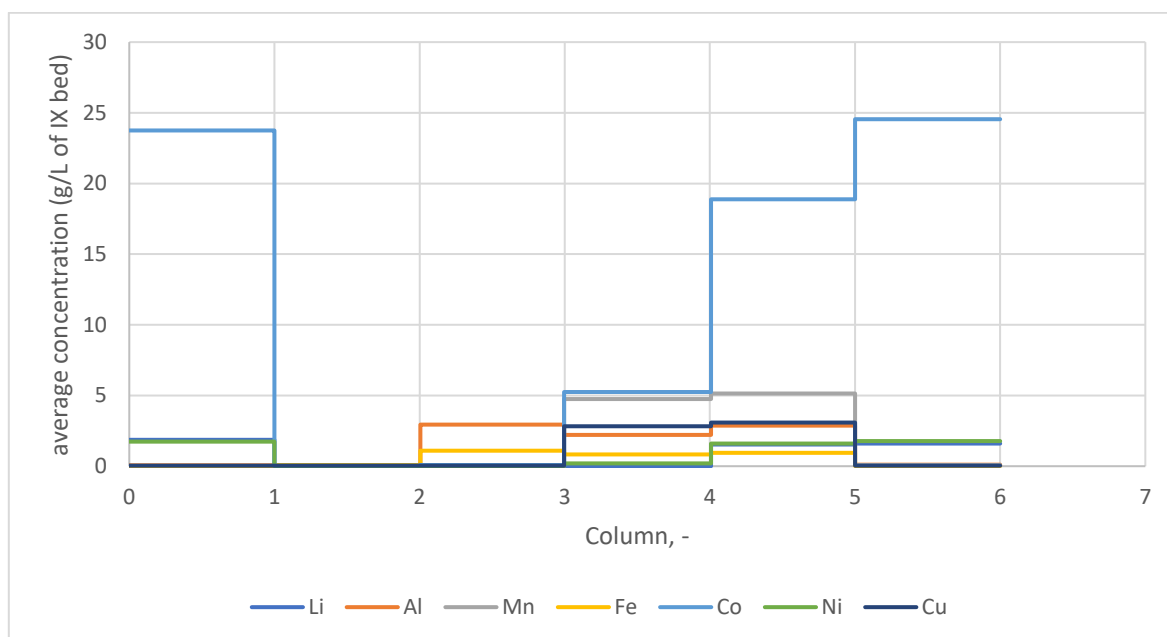


Figure 38 Solid and liquid phase axial profile after switch 20 in SMB 2

The recoveries of the metals in different steps are presented in Table XXI. As can be seen, up to 13 % of cobalt is lost to extract 1 but only 3.66 % of nickel, which are far better than the losses in SMB 1. The purities of the outlets are presented in Table XXII. The purity of raffinate is 99.86 %, so no undesired metals are in it. The impurity of extract 1 is lower than in SMB 1 due to the large amount of cobalt and aluminium in it.

Table XXI Single-metal recoveries in raffinate, extract 1 and extract 2 in experiment SMB 2

		Li	Al	Mn	Fe	Co	Ni	Cu
Raffinate		95.36	0.45	0.25	0.20	82.01	91.27	0.03
recovery, %								
Extract	1	0.25	15.69	100.03	3.98	13.47	3.66	100.4
recovery, %								
Extract	2	0	78.97	0.35	92.0	0.29	0.34	0.31
recovery, %								

Table XXII Raffinate, extract 1 and extract 2 purities in experiment SMB 2

Raffinate (Co, Li, Ni), %	99.86
Extract 1 (Cu, Mn), %	58.53
Extract 2 (Fe, Al), %	96.55

8.3 SMB 3

The third SMB experiment, SMB 3, was based on the results received from SMB 2. All the parameters were based on those experiments and are presented in Table XXIII.

The duration of the experiment was chosen to be 24 switches to make sure that the process would be in steady state. Due to the cobalt and nickel losses in SMB 2, the multi metal solution feed was still increased to 2.5 BV to hopefully achieve a complete elution of Co.

Table XXIII Parameters of experiment SMB 3

Switch time, min	25
Temperature, C	60
Multi metal solution pH, -	1.8
Number of switches completed	24
Multi metal solution feed, BV	2.5
Elution feed, BV	1.5
Desorption 1 feed, BV	2.5
Desorption 2 feed, BV	4.0
Regeneration feed, BV	1.5
Multi metal solution flowrate, BV/h	6.0
Elution flowrate, BV/h	3.6
Desorption 1 flowrate, BV/h	6.0
Desorption 2 flowrate, BV/h	13.2
Regeneration flowrate, BV/h	13.2
Duration of the experiment, h	10

All of the three outlets, raffinate, extract 1 and extract 2 were sampled as aggregate samples, meaning that one switch yielded one sample since they were not fractionated. Switch 24 was fractionated in all three samples to see if the copper and manganese break through, when it would happen. The copper and manganese ultimately did not break through in the raffinate. After the experiment was over, the columns were desorbed with desorbent 1 and desorbent 2 to compile a solid and liquid phase axial profile to more accurately find out how the metals that present in each column after every phase of the process.

8.3.1 SMB 3 results

The results of the raffinate samples analyzed from switches 1-23 are presented in Figure 39. It can be seen that the cobalt content in the samples is almost at the same rate as other target metals.

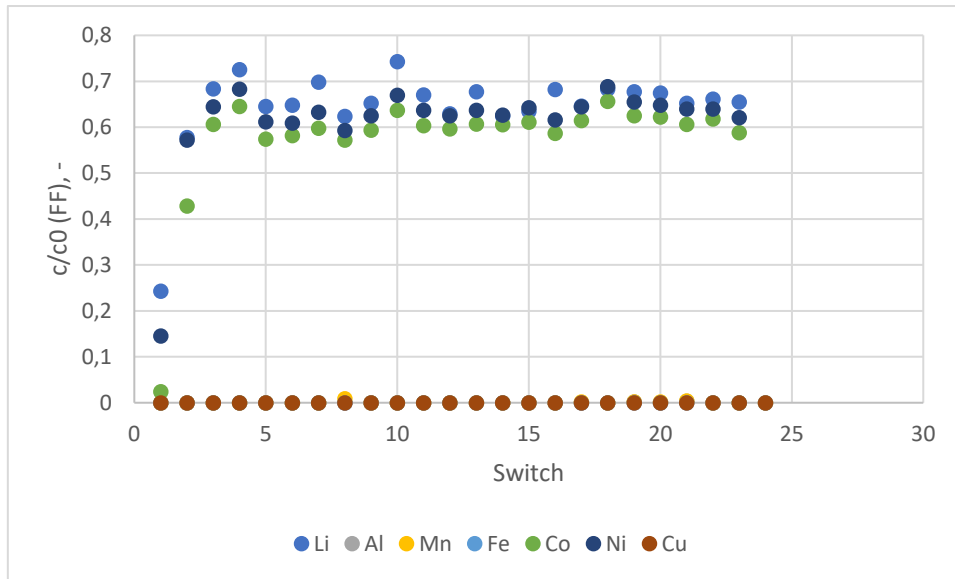


Figure 39 ICP analysis of switch 1-23 of raffinate in SMB 3 from aminomethylphosphonic acid functional Lewatit MDS TP260 resin. $T = 60^{\circ}\text{C}$. Loading flowrate 6 BV/h, elution flowrate 3.6 BV/h. Flow direction top to bottom. Eluent used 1.8 pH H_2SO_4 .

The results of the extract 1 samples analyzed from switches 1-23 are presented in Figure 40. It can be seen from the Figure, that in addition to manganese and copper, the desired metals to be desorbed in this step, some cobalt and aluminium are also desorbed, though very little cobalt is desorbed.

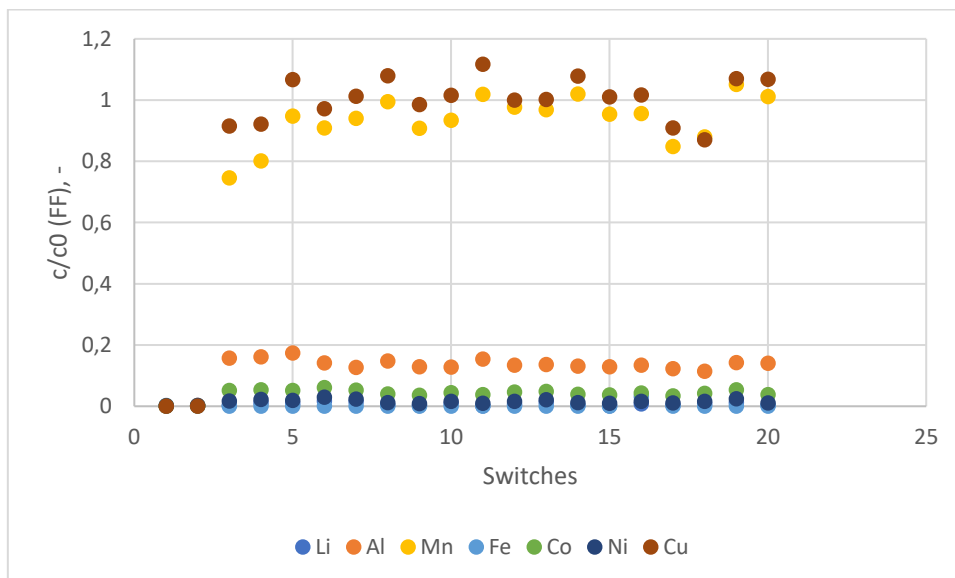


Figure 40 ICP analysis of switches 1-23 of extract 1 in SMB 3. Desorption from aminomethylphosphonic acid functional Lewatit MDS TP260 resin. $T = 60^{\circ}\text{C}$. Flowrate 6 BV/h. Flow direction top to bottom. Desorbent used 1 M H_2SO_4 .

The results of the extract 2 samples analyzed from switches 1-23 are presented in Figure 41. In this step, desorption 2 and regeneration are combined. It can be seen from the Figure that only iron and aluminium are desorbed at this step, which means that all the other metals were desorbed successfully at previous steps.

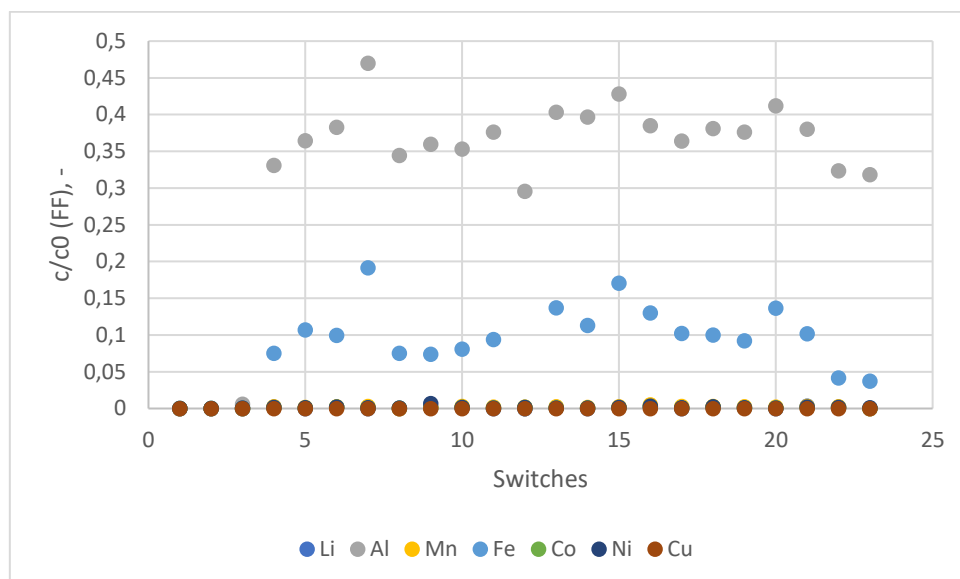


Figure 41 ICP analysis of extract 2 switches 1-23 in SMB 3. Desorption from aminomethylphosphonic acid functional Lewatit MDS TP260 resin. $T = 60^{\circ}\text{C}$. Flowrate of Desorption 2 and regeneration 13.2 BV/h. Flow direction top to bottom. Desorbent used 0.4 M $\text{K}_2\text{-oxalate}$, regenerate used 1 M H_2SO_4 .

The axial profile of SMB 3 is presented in Figure 42. This Figure is after switch 24 is completed and switch 25 should start next with a new cycle. There are no metals in column 6, which has just been regenerated, and only iron and aluminium in column 1, which has just been in desorption 1. As expected, column 3 contains all the metals, since multi metal solution has been fed into it, and columns 4 and 5 contain the target metals, lithium, nickel and cobalt. Column 2 has just been eluted, and it should not contain any of the target metals, but as can be seen, little cobalt is still left in the column, so its recovery in the raffinate will not be perfect. It can also be seen that very little copper had travelled to column 4, which could mean that the process had not achieved steady state after the 24 switches it was run for, and if it was run for much longer copper could get in to the raffinate, making it impure.

The feed of 2.5 BV of multi metal solution to the process may be over the limit of the ion exchange capacity.

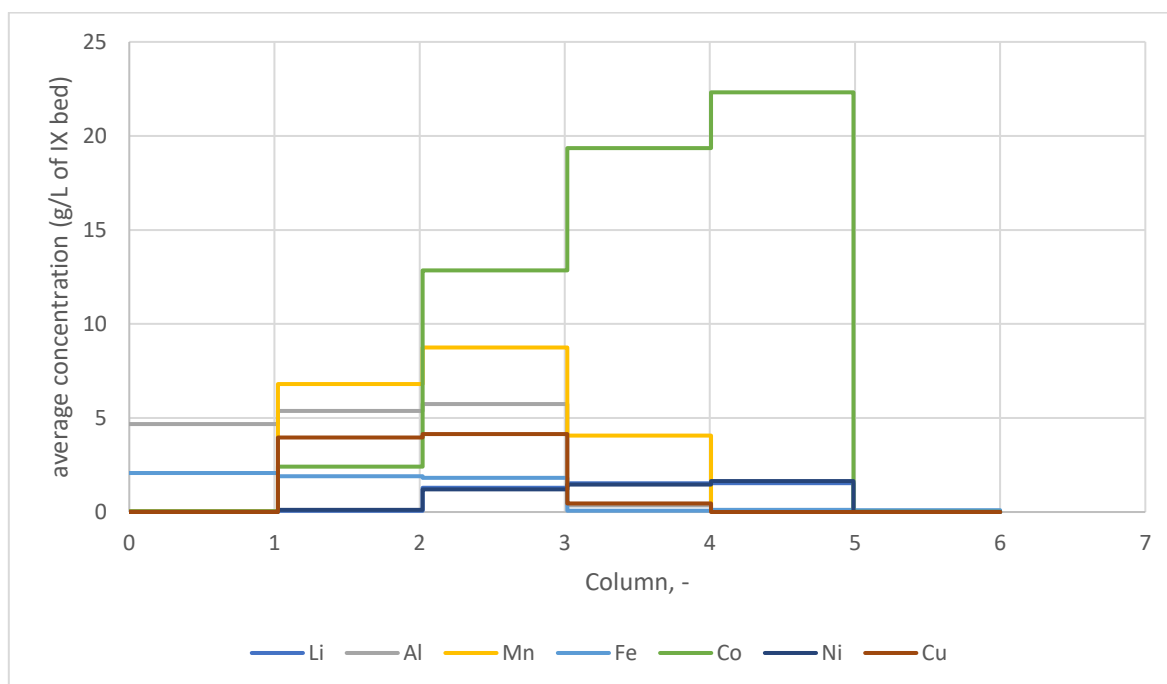


Figure 42 Solid and liquid phase axial profile after switch 24 in SMB 3

The recoveries of the metals in different steps are presented in Table XXIV. As can be seen, only 3.58 % of cobalt is lost to extract 1 and only 1,2 % of nickel, which are far better than the losses in SMB 1 and SMB 2. The purities of the outlets are presented in Table XXV. The purity of raffinate is 99.91 %, so no undesired metals are in it. The impurity of extract 1 is higher than in previous experiments at 78.60 % due to the lower loss of cobalt to extract 1.

Table XXIV Single-metal recoveries in raffinate, extract1 and extract 2 in experiment SMB 3

	Li	Al	Mn	Fe	Co	Ni	Cu
Raffinate recovery, %	99.09	0.20	0.28	0.12	91.34	95.61	0
Extract 1 recovery, %	0.41	12.26	86.89	0.66	3.58	1.18	91.40
Extract 2 recovery, %	0.30	65.81	0.39	74.87	0.15	0.23	0

Table XXV Raffinate, extract 1 and extract 2 purities in experiment SMB 3

Raffinate (Co, Li, Ni), %	99.94
Extract 1 (Cu, Mn), %	78.60
Extract 2 (Fe, Al), %	96.48

8.4 Discussion regarding the SMB experiments

The process was able to be improved over the three SMB experiments conducted. The purities of the raffinate, extract 1 and extract 2 over experiments SMB 1, SMB 2 and SMB 3 are presented in Table XXVI.

Table XXVI Raffinate, extract 1 and extract 2 purities of experiments SMB 1, SMB 2 and SMB 3

	SMB 1	SMB 2	SMB 3
Raffinate (Co, Li, Ni), %	99.46	99.85	99.94
Extract 1 (Cu, Mn), %	69.42	58.53	78.46
Extract 2 (Fe, Al), %	96.56	96.54	96.48

As can be seen from the Table, the purity of the raffinate improved over the experiments, although having been over 99.4 % in all three experiments. The greatest advances were made in the amount of cobalt lost to extract 1 during desorption 1, which is reflected in the purity of extract 1 increasing over the experiments. The extract 2 purity did not improve much over the experiments, remaining at about 96 %.

The main problem in the SMB process was the loss of target metals to extract 1. The losses of cobalt and nickel to extract 1 over experiments SMB 1, SMB 2 and SMB 3 are presented in Table XXVII.

Table XXVII Co and Ni losses in experiments SMB 1, SMB 2 and SMB 3

	SMB 1	SMB 2	SMB 3
Co loss, %	43.74	13.78	3.57
Ni loss, %	14.65	3.56	1.18

As can be seen from the Table, the loss of cobalt reduced to 3.6 % in SMB 3 from 43.7 % in SMB 1, making a great improvement. The loss of nickel also reduced to 1.2 % in SMB 3 from 14.7 % in SMB 1.

The improvements in the SMB were achieved by increasing the amount of multi metal solution fed into the process, meaning that the productivity of the process also increased.

When compared to other hydrometallurgical processes, the amount of lost metals is extremely low. Precipitation as a metal separation method results in losses of 29 % of lithium and 5.3 % of cobalt. Solvent extraction results in 10 % losses of both nickel and cobalt. The final single column process developed in the single column experiments loses 5.92 % of cobalt, which is significantly higher than the amount lost in SMB 3, although the process was not fully optimized.

9 CONCLUSIONS

The recycling of Li-ion batteries is extremely important not only to keep toxic waste out of our landfills and prevent it from harming nature, wildlife or humans, but recycling of them is a great way to source valuable metals like cobalt, nickel and lithium for a continuously and rapidly growing demand. Batteries are needed for large-scale items like electric vehicles as we are seeing a transition to more climate-conscious ways to travel, but also to small electronic devices, like phones and cameras.

Ion exchange is a great way to separate cobalt, lithium, and nickel from other metals in Li-ion battery waste leachate, and it could also be possible to develop a process where all the target metals are separated individually, not to a mix of metals.

The SMB process demonstrated in this Thesis allows for a higher product yield, better efficiency, and larger producing scale than a single column batch process. As a continuous process, the SMB can also be more economical, uses less expensive solutions like desorbents and demands less labor to operate.

The process demonstrated in this thesis can operate with a 99.91 % raffinate purity. It can also recover most of the target metals, losing only 0.41 % of lithium, 1.41 % of nickel and 3.58 % of cobalt. Other typical hydrometallurgical methods like precipitation result in 29 % loss of lithium and 5.3 % loss of cobalt. Solvent extraction also results in 10 % losses of both nickel and cobalt.

REFERENCES

- Guiral, J. 2018. Textural and mineralogical characterization of Li-pegmatite deposit: Using microanalytical and image analysis to link micro and macro properties of Spodumene in drill cores Keliber Lithium Project, Finland. Available: https://www.researchgate.net/publication/327160488_Textural_and_mineralogical_characterization_of_Li-pegmatite_deposit_Using_microanalytical_and_image_analysis_to_link_micro_and_macro_properties_of_Spodumene_in_drill_cores_Keliber_Lithium_Project_Finl. Accessed 2.2.2023.
- Amilton Barbosa Botelho Junior, André de Albuquerque Vicente, Denise Crocce Romano Espinosa, Jorge Alberto Soares Tenório. 2019. Recovery of metals by ion exchange process using chelating resin and sodium dithionite. *Journal of Materials Research and Technology*, Volume 8, Issue 5, 2019, Pages 4464-4469, ISSN 2238-7854, <https://doi.org/10.1016/j.jmrt.2019.07.059>. Available: (<https://www.sciencedirect.com/science/article/pii/S2238785418312110>)
- Baum, Z. 2022. Lithium-Ion Battery Recycling—Overview of Techniques and Trends. Available: <https://pubs.acs.org/doi/10.1021/acsenergylett.1c02602>. Accessed 1.2.2023.
- Chagnes, A. & Pospiech, B. (2013) A brief review on hydrometallurgical technologies for recycling spent lithium-ion batteries. *Journal of chemical technology and biotechnology* (1986). [Online] 88 (7), 1191–1199. Accessed 4.8.2023.
- Chawla, N. 2019. Recent Advances in Non-Flammable Electrolytes for Safer Lithium-Ion Batteries. Available: https://www.researchgate.net/publication/330798113_Recent_Advances_in_Non-Flammable_Electrolytes_for_Safer_Lithium-Ion_Batteries. Accessed 16.11.2022.
- ChemBK. 2022. Sodium oxalate - Physico-chemical Properties. Available: <https://www.chembk.com/en/chem/Sodium%20oxalate>. Accessed 5.2.2023.
- Domenech et al. 2012. Bifunctional Polymer-Metal Nanocomposite Ion Exchange Materials. Available: <https://www.intechopen.com/chapters/40701>. Accessed: 3.3.2023.
- Earth Org. 2023. The Environmental Impacts of Cobalt Mining in Congo. Available: <https://earth.org/cobalt-mining-in-congo/>. Accessed 1.4.2023.
- Electrive. 2023. Ecobat builds new Li-ion battery recycling plant in the US. Available: <https://www.electrive.com/2023/02/22/ecobat-builds-third-li-ion-battery-recycling-plant-in-the-usa/>- Accessed: 15.6.2023.

European Commission. 2023. Critical raw materials. Available: https://single-market-economy.ec.europa.eu/sectors/raw-materials/areas-specific-interest/critical-raw-materials_en. Accessed 12.3.2023.

Fischer Scientific. 2023. Available: <https://www.fishersci.com/shop/products/lewatit-tp-260-disodium-form-milliporesigma-supelco/111004458>. Accessed 5.4.2023.

Fleming C., McMullen J., Thomas K., Wells J. 2003. Recent advances in the development of an alternative to the cyanidation process: thiosulphate leaching and resin in pulp, *Miner. Metal. Proc.* 20(1): 1–9. Accessed 5.8.2023.

IEA. 2023. (a) Trends in batteries. Available: <https://www.iea.org/reports/global-ev-outlook-2023/trends-in-batteries>. Accessed 15.3.2023.

IEA. 2023. (b) Critical Minerals Market Review 2023. Available: <https://iea.blob.core.windows.net/assets/afc35261-41b2-47d4-86d6-d5d77fc259be/CriticalMineralsMarketReview2023.pdf>. Accessed 5.8.2023.

Larouche et al. 2020. Progress and Status of Hydrometallurgical and Direct Recycling of Li-Ion Batteries and Beyond. Available: https://scholar.google.fi/scholar_url?url=https://www.mdpi.com/1996-1944/13/3/801/pdf&hl=sv&sa=X&ei=v9rPZJuuMZCay9YP2OCXiAs&scisig=AFWwaeaSLuPoSvabpZ_SrhBUaPE9&oi=scholarr. Accessed 12.6.2023.

Lenntech. 2019. (a). PRODUCT INFORMATION LEWATIT® MonoPlus TP 260. Available: [lenntech.com/Data-sheets/Lewatit-MonoPlus-TP-260-EN-L.pdf](https://www.lenntech.com/Data-sheets/Lewatit-MonoPlus-TP-260-EN-L.pdf). Accessed: 15.11.2022.

Lenntech. 2019. (b). PRODUCT INFORMATION LEWATIT® MDS TP 260. Available: <https://www.lenntech.com/Data-sheets/Lewatit-MDS-TP-260-EN-L.pdf>. Accessed: 5.3.2023.

Lopes et al. 2012. Ion Exchange Technology II: Metal Recovery, Separation and/or Pre-concentration. Available: https://link-springer-com.ezproxy.cc.lut.fi/chapter/10.1007/978-94-007-4026-6_11#Sec1. Accessed 13.11.2022.

Nasef, M. 2012. Introduction to Ion Exchange Processes. Available: https://link-springer-com.ezproxy.cc.lut.fi/chapter/10.1007/978-94-007-1700-8_1. Accessed: 16.11.2023.

PharmaTech. 2007. Simulated Moving Bed Chromatography: A Powerful Unit Operation. Available: https://www.pharmatech.com/view/simulated-moving-bed-chromatography-powerful-unit-operation_ Accessed 3.5.2023.

- Porvali, A. 2019. Mechanical and hydrometallurgical processes in HCl media for the recycling of valuable metals from Li-ion battery waste. Available: <https://www.sciencedirect-com.ezproxy.cc.lut.fi/science/article/pii/S092134491830449X?via%3Dihub>. Accessed 7.11.2022.
- Ramkumar, J. 2012. Principles of Ion Exchange Equilibria. Available: https://link.springer.com/chapter/10.1007/978-94-007-1700-8_2. Accessed 8.5.2023.
- RecycLiCo. 2023. Available: recyclico.com/technology. Accessed 6.5.2023.
- Rietveld, E. GLOBAL ENERGY TRANSITION AND METAL DEMAND. Available: https://www.researchgate.net/publication/330468693_GLOBAL_ENERGY_TRANSITION_AND_METAL_DEMAND. Accessed 6.1.2023.
- Rodrigues et al. 2015. SIMULATED MOVING BED TECHNOLOGY. Available: <https://core.ac.uk/download/pdf/153413515.pdf>. Accessed: 1.12.2022.
- Sigma Aldrich. 2022. Available: <https://www.sigmaaldrich.com/FI/en/product/sial/62103>. Accessed 22.11.2022.
- Silva et al. 2012. Use of Ion Exchange Resins in Continuous Chromatography for Sugar Processing. Available: https://link-springer-com.ezproxy.cc.lut.fi/chapter/10.1007/978-94-007-4026-6_5#Abs1. Accessed 6.12.2022.
- Sharma, D. 2021. Simulated Moving Bed Technology: Overview and Use in Biorefineries. Available: https://www.researchgate.net/publication/354894224_Simulated_Moving_Bed_Technology_Overview_and_Use_in_Biorefineries/link/6153227d154b3227a8b6e38e/download. Accessed: 3.4.2023.
- Singh, P. 2019. Energy Storage Systems for Electric Vehicles. Available: https://www.researchgate.net/publication/343746458_Energy_Storage_Systems_for_Electric_Vehicles. Accessed 5.12.2022.
- Sobianowska-Turek, A. The Necessity of Recycling of Waste Li-Ion Batteries Used in Electric Vehicles as Objects Posing a Threat to Human Health and the Environment. Available: https://www.researchgate.net/publication/352058721_The_Necessity_of_Recycling_of_Waste_Li-Ion_Batteries_Used_in_Electric_Vehicles_as_Objects_Posing_a_Threat_to_Human_Health_and_the_Environment. Accessed 20.11.2022.
- Sole, K., Mooiman, M., Hardwick, E. 2016. (a). Present and future applications of ion exchange in hydrometallurgy: An overview. Available: https://www.researchgate.net/publication/305462927_Present_and_future_applications_of_ion_exchange_in_hydrometallurgy_An_overview. Accessed 4.8.2023.

Sole K., Hardwick E., Prinsloo A. 2016. (b). Recovery of copper from Chilean mine waste waters, in International Mine Waters Association Conference 2016, Leipzig, in press. Accessed 2.8.2023.

Tang Y-C, Wang J-Z and Shen Y-H. 2023. Separation of Valuable Metals in The Recycling of Lithium Batteries via Solvent Extraction Minerals 13 285 Online: <http://dx.doi.org/10.3390/min13020285>. Accessed: 3.8.2023.

Toumi, A., Engell, S., Diehl, M., Bock, H.G., Schlöder, J. 2007. Efficient optimization of simulated moving bed processes, Chemical Engineering and Processing: Process Intensification, vol. 46, no. 11, s. 1067-1084. Accessed 15.11.2022.

Umicore. 2023. Umicore Battery Recycling: Capturing profitable growth and enabling a circular and low-carbon battery value chain. Available: [umicore.com/en/newsroom/umicore-battery-recycling](https://www.umicore.com/en/newsroom/umicore-battery-recycling). Accessed 4.6.2023.

U.S. Department of Energy Office of Scientific and Technical Information. 2023. Lithium-ion battery recycling processes: Research towards a sustainable course. Available: <https://www.osti.gov/biblio/1558994>. Accessed: 7.6.2023.

Virolainen, S., Wesselborg, T., Sainio, T. 2021. Removal of iron, aluminium, manganese and copper from leach solutions of lithium-ion battery waste using ion exchange. Available: https://www.researchgate.net/publication/351033638_Removal_of_iron_aluminium_manganese_and_copper_from_leach_solutions_of_lithium-ion_battery_waste_using_ion_exchange. Accessed: 29.11.2022.

Wang, D. 2019. Soft Sensing Modeling of the SMB Chromatographic Separation Process Based on the Adaptive Neural Fuzzy Inference System. Available: https://www.researchgate.net/publication/337237654_Soft_Sensing_Modeling_of_the_SMB_Chromatographic_Separation_Process_Based_on_the_Adaptive_Neural_Fuzzy_Inference_System/link/61827babeef53e51e121709e/download. Accessed 4.3.2023.

Yoshida et al. 1985. KINETICS IN A CHELATE ION EXCHANGER-I. THEORETICAL ANALYSIS . Available: https://d1wqtxts1xzle7.cloudfront.net/69654667/0009-2509_2886_2980036-720210914-26529-ut978e-libre.pdf?1631653666=&response-content-disposition=inline%3B+filename%3DKinetics_in_a_chelate_ion_exchanger_I_Th.pdf&Expires=1691350595&Signature=G3aTcuUf040UqBlqgtLD~1nDKCWw-nuEz1TQelt4PLOtoUCIIDewkwi8~sWc0nf5ZuTqUv-Bzi9KNJN3r2qTJekWTJH7PWbEzfzIzEpc5HXxVVzFrLidgYzjUyo-o8noLUobNnVQOCLkuILyOH8w4NiO98pbOHfeTLfM~YvXYTzJVwPYB-n4U4GvuOsvMPIjGwvSZapBMPdPSztvXRqNZ6UjqwvcWLjBjjsrkd67X-L~-

xwx4omLW5zhjTg52GJ41~mEkmCPVjy5Q4l-
mtXLpIaLKRcoz3c7gWrzkqBGxRhazCYeyM~M4ex7Tz8qiNKvgyDirb7Uy0ds2GAm9LOk4A__
&Key-Pair-Id=APKAJLOHF5GGSLRBV4ZA. Accessed: 3.8.2023.

Shu-guang ZHU, Wen-zhi HE, Guang-ming LI, Xu ZHOU, Xiao-jun ZHANG, Ju-wen HUANG.
2012. Recovery of Co and Li from spent lithium-ion batteries by combination method of acid
leaching and chemical precipitation, Transactions of Nonferrous Metals Society of China, Volume
22, Issue 9, 2012, Pages 2274-2281, ISSN 1003-6326, [https://doi.org/10.1016/S1003-6326\(11\)61460-X](https://doi.org/10.1016/S1003-6326(11)61460-X).
(<https://www.sciencedirect.com/science/article/pii/S100363261161460X>). Accessed 1.6.2023.

APPENDICES

Appendix I

Parameters of single column experiments

Table XXVIII C1 Parameters

Date:	12.-13.12.2022				
Aim:	Column test run				
Experiment:	C1				
Column:	New				
Loading:	V injected:	8 BV			
	t injection:	240 min			
	Flowrate:	2 BV/h			
	Flow direction:	bottom to top			
	Autosampler:	t initial:	600 s		
		t valve on :	120 s		
		t valve off:	10 s		
	Conductivity:	1000 mS/cm			
	UV:	I1 = 260 I2 = 240			
	RI:				
Last sample:	L106				
Elution:	Flowrate:	6 BV/h			
	Flow direction:	bottom to top			
	Autosampler:	t valve on :	120 s		
		t valve off:	10 s		
Desorption 1:	V injected:	4 BV			
	t injection:	120 min			
	Flowrate:	6 BV/h			
	Flow direction:	top to bottom			
	Autosampler:	t initial:	600 s		
		t valve on :	120 s		
		t valve off:	10 s		
	Conductivity:	1000 mS/cm			
	UV:	I1 = 260 I2 = 240			
	RI:				
Last sample:					
Desorption 2	V injected:	4 BV			
	t injection:	120 min			
	Flowrate:	6 BV/h			
	Flow direction:	top to bottom			
	Autosampler:	t initial:	600 s		
		t valve on :	120 s		
		t valve off:	10 s		
	Conductivity:	1000 mS/cm			
	UV:	I1 = 260 I2 = 240			
	RI:				
Last sample:					
Regeneration:	V injected:	2 BV			
	t injection:	60 min			
	Flowrate:	6 BV/h			
	Flow direction:	top to bottom			
	Autosampler:	t initial:	600 s		
		t valve on :	120 s		
	t valve off:	10 s			

Table XXIX C2 Parameters

Date:	16.1.2023			
Aim:	H2SO4 removal from column with 0,85 M Na2SO4			
Experiment:	C2			
Column:	New			
Desorption 2:	V injected:	1 BV		
	t injection:	10 min		
	Flowrate:	6 BV/h		
	Flow direction:	top to bottom		
	Autosampler:	t initial:		
		t valve on :		no samples
		t valve off:		
	Conductivity:	1000 mS/cm		
	UV:	I1 =	260	I2 =
	RI:			
Last sample:				
Regeneration:	V injected:	2,5 BV		
	t injection:	25 min		
	Flowrate:	6 BV/h		
	Flow direction:	top to bottom		
	Autosampler:	t valve on :		no samples
		t valve off:		
0,85 M Na2SO4:	V injected:	4 BV		
	t injection:	40 min		
	Flowrate:	6 BV/h		
	Flow direction:	bottom to top		
	Autosampler:	t initial:	200 s	
		t valve on :	120 s	
		t valve off:	10 s	
	Conductivity:	1000 mS/cm		
	UV:	I1 =	260	I2 =
	RI:			
Last sample:				

Table XXX C5 Parameters

Date:	19.1.2023				
Aim:	Fe-solution test, feed 0,5 BV				
Experiment:	C5				
Column:	Old				
Loading:	V injected:	0,5 BV			
	t injection:	5 min			
	Flowrate:	6 BV/h			
	Flow direction:	bottom to top			
	Autosampler:	t initial:			
		t valve on :		no samples	
		t valve off:			
	Conductivity:	1000 mS/cm			
	UV:	I1 =	350	I2 =	240
	RI:				
	Last sample:				
Desorption 2:	V injected:	4 BV			
	t injection:	40 min			
	Flowrate:	6 BV/h			
	Flow direction:	top to bottom			
	Autosampler:	t initial:	0 s		
		t valve on :	120 s		
		t valve off:	10 s		
	Conductivity:	1000 mS/cm			
	UV:	I1 =	350	I2 =	240
	RI:				
	Last sample:				
Regeneration:	V injected:	2 BV			
	t injection:	20 min			
	Flowrate:	6 BV/h			
	Flow direction:	top to bottom			
	Autosampler:	t initial:			
		t valve on :		no samples	
		t valve off:			
	Conductivity:	1000 mS/cm			
	UV:	I1 =	350	I2 =	240
	RI:				
	Last sample:				

Table XXXI C6 Parameters

Date:	19.1.2023			
Aim:	Fe-solution test, feed 1 BV			
Experiment:	C6			
Column:	Old			
Loading:	V injected:	1 BV		
	t injection:	10 min		
	Flowrate:	6 BV/h		
Flow direction:	bottom to top			
Autosampler:	t initial:			
	t valve on :	no samples		
	t valve off:			
Conductivity:	1000 mS/cm			
UV:	l1 =	350	l2 =	240
RI:				
Last sample:				
Desorption 2:	V injected:	4 BV		
	t injection:	40 min		
	Flowrate:	6 BV/h		
Flow direction:	top to bottom			
Autosampler:	t initial:	0 s		
	t valve on :	120 s		
	t valve off:	10 s		
Conductivity:	1000 mS/cm			
UV:	l1 =	350	l2 =	240
RI:				
Last sample:				
Regeneration:	V injected:	2 BV		
	t injection:	20 min		
	Flowrate:	6 BV/h		
Flow direction:	top to bottom			
Autosampler:	t initial:			
	t valve on :	no samples		
	t valve off:			
Conductivity:	1000 mS/cm			
UV:	l1 =	350	l2 =	240
RI:				
Last sample:				

Table XXXII C7 Parameters

Date:	19.1.2023				
Aim:	Fe-solution test, feed 1,5 BV				
Experiment:	C7				
Column:	Old				
Loading:	V injected:	1,5 BV			
	t injection:	15 min			
	Flowrate:	6 BV/h			
	Flow direction:	bottom to top			
Autosampler:	t initial:				
	t valve on :		no samples		
	t valve off:				
	Conductivity:	1000 mS/cm			
UV:	l1 =	350	l2 =	240	
RI:					
Last sample:					
Desorption 2:	V injected:	4 BV			
	t injection:	40 min			
	Flowrate:	6 BV/h			
	Flow direction:	top to bottom			
Autosampler:	t initial:	0 s			
	t valve on :	120 s			
	t valve off:	10 s			
	Conductivity:	1000 mS/cm			
UV:	l1 =	350	l2 =	240	
RI:					
Last sample:					
Regeneration:	V injected:	2 BV			
	t injection:	20 min			
	Flowrate:	6 BV/h			
	Flow direction:	top to bottom			
Autosampler:	t initial:				
	t valve on :		no samples		
	t valve off:				
	Conductivity:	1000 mS/cm			
UV:	l1 =	350	l2 =	240	
RI:					
Last sample:					

Table XXXIII C8 Parameters

Date:	19.1.2023			
Aim:	Fe-solution test, feed 2,5 BV			
Experiment:	C8			
Column:	Old			
Loading:	V injected:	2,5 BV		
	t injection:	25 min		
	Flowrate:	6 BV/h		
Flow direction:	bottom to top			
Autosampler:	t initial:			
	t valve on :			no samples
	t valve off:			
Conductivity:	1000 mS/cm			
UV:	l1 =	350	l2 =	240
RI:				
Last sample:				
Desorption 2: 0,2 M Na-oxalate	V injected:	4 BV		
	t injection:	40 min		
	Flowrate:	6 BV/h		
Flow direction:	top to bottom			
Autosampler:	t initial:	0 s		
	t valve on :	120 s		
	t valve off:	10 s		
Conductivity:	1000 mS/cm			
UV:	l1 =	350	l2 =	240
RI:				
Last sample:				
Regeneration:	V injected:	2 BV		
	t injection:	20 min		
	Flowrate:	6 BV/h		
Flow direction:	top to bottom			
Autosampler:	t initial:			
	t valve on :			no samples
	t valve off:			
Conductivity:	1000 mS/cm			
UV:	l1 =	350	l2 =	240
RI:				
Last sample:				

Table XXXIV C9 Parameters

Date:	20.1.2023			
Aim:	Fe-solution test, feed 2,5 BV			
Experiment:	C9			
Column:	Old			
Loading:	V injected:	2,5 BV		
	t injection:	25 min		
	Flowrate:	6 BV/h		
Flow direction:	bottom to top			
Autosampler:	t initial:			
	t valve on :	no samples		
	t valve off:			
Conductivity:	1000 mS/cm			
UV:	l1 =	350	l2 =	240
RI:				
Last sample:				
Desorption 2: 0,4 M K-oxalate	V injected:	4 BV		
	t injection:	40 min		
	Flowrate:	6 BV/h		
Flow direction:	top to bottom			
Autosampler:	t initial:	0 s		
	t valve on :	120 s		
	t valve off:	10 s		
Conductivity:	1000 mS/cm			
UV:	l1 =	350	l2 =	240
RI:				
Last sample:				
Regeneration:	V injected:	2 BV		
	t injection:	20 min		
	Flowrate:	6 BV/h		
Flow direction:	top to bottom			
Autosampler:	t initial:			
	t valve on :	no samples		
	t valve off:			
Conductivity:	1000 mS/cm			
UV:	l1 =	350	l2 =	240
RI:				
Last sample:				

Table XXXV C10 Parameters

Date:	20.1.2023			
Aim:	Fe-solution test, feed 4,5 BV			
Experiment:	C10			
Column:	Old			
Loading:	V injected:	4,5 BV		
	t injection:	45 min		
	Flowrate:	6 BV/h		
	Flow direction:	bottom to top		
	Autosampler:	t initial:		
		t valve on :	no samples	
		t valve off:		
	Conductivity:	1000 mS/cm		
	UV:	l1 =	350	l2 = 240
	RI:			
	Last sample:			
Desorption 2: 0,2 M Na-oxalate	V injected:	4 BV		
	t injection:	40 min		
	Flowrate:	6 BV/h		
	Flow direction:	top to bottom		
	Autosampler:	t initial:	0 s	
		t valve on :	120 s	
		t valve off:	10 s	
	Conductivity:	1000 mS/cm		
	UV:	l1 =	350	l2 = 240
	RI:			
	Last sample:			
Regeneration:	V injected:	2 BV		
	t injection:	20 min		
	Flowrate:	6 BV/h		
	Flow direction:	top to bottom		
	Autosampler:	t initial:		
		t valve on :	no samples	
		t valve off:		
	Conductivity:	1000 mS/cm		
	UV:	l1 =	350	l2 = 240
	RI:			
	Last sample:			

Table XXXVI C11 Parameters

Date:	20.1.2023			
Aim:	Fe-solution test, feed 6 BV			
Experiment:	C11			
Column:	Old			
Loading:	V injected:	6 BV		
	t injection:	60 min		
	Flowrate:	6 BV/h		
	Flow direction:	bottom to top		
Autosampler:	t initial:			
	t valve on :	no samples		
	t valve off:			
	Conductivity:	1000 mS/cm		
UV:	l1 =	350	l2 =	240
RI:				
Last sample:				
Desorption 2:	V injected:	4 BV		
0,2 M Na-oxalate	t injection:	40 min		
	Flowrate:	6 BV/h		
	Flow direction:	top to bottom		
Autosampler:	t initial:	0 s		
	t valve on :	120 s		
	t valve off:	10 s		
	Conductivity:	1000 mS/cm		
UV:	l1 =	350	l2 =	240
RI:				
Last sample:				
Regeneration:	V injected:	2 BV		
	t injection:	20 min		
	Flowrate:	6 BV/h		
	Flow direction:	top to bottom		
Autosampler:	t initial:			
	t valve on :	no samples		
	t valve off:			
	Conductivity:	1000 mS/cm		
UV:	l1 =	350	l2 =	240
RI:				
Last sample:				

Table XXXVII C13 Parameters

Date:	30.1.2023					
Aim:	TP20 resin, SMB settings, 100 % multi metal solution					
Experiment:	C13					
Column:	Old					
Loading:	V injected:	2,5 BV				
	t injection:	25 min				
	Flowrate:	6 BV/h				
	Flow direction:	bottom to top				
	Autosampler:	t initial:	200 s			
		t valve on :	120 s			
		t valve off:	10 s			
Conductivity:	1000 mS/cm					
UV:	l1 =	260	l2 = 240			
RI:						
Last sample:	C13 L10					
Elution:	V injected:	1,5 BV				
	t injection:	25 min				
	Flowrate:	3,6 BV/h				
	Flow direction:	bottom to top				
	Autosampler:	t initial:	333 s			
		t valve on :	120 s			
		t valve off:	10 s			
Last sample:	C13 E9					
Desorption 1	V injected:	2,5 BV				
	t injection:	25 min				
	Flowrate:	6 BV/h				
	Flow direction:	top to bottom				
	Autosampler:	t initial:	200 s			
		t valve on :	120 s			
		t valve off:	10 s			
Conductivity:	1000 mS/cm					
UV:	l1 =	260	l2 = 240			
RI:						
Last sample:	C13 D1 10					
Desorption 2	V injected:	2,5 BV				
	t injection:	25 min				
	Flowrate:	6 BV/h				
	Flow direction:	top to bottom				
	Autosampler:	t initial:	200 s			
		t valve on :	120 s			
		t valve off:	10 s			
Conductivity:	1000 mS/cm					
UV:	l1 =	260	l2 = 240			
RI:						
Last sample:	C13 D2 10					
Regeneration:	V injected:	1 BV				
	t injection:	25 min				
	Flowrate:	2,4 BV/h				
	Flow direction:	top to bottom				
	Autosampler:	t initial:	250 s			
		t valve on :	120 s			
		t valve off:	10 s			
Last sample:	C13 RE 7					

Table XXXVIII C14 Parameters

Date:	30.1.2023					
Aim:	TP20 resin, SMB settings, 50 % multi metal solution					
Experiment:	C14					
Column:	Old					
Loading:	V injected:	2,5 BV				
	t injection:	25 min				
	Flowrate:	6 BV/h				
	Flow direction:	bottom to top				
	Autosampler:	t initial:	200 s			
		t valve on :	120 s			
		t valve off:	10 s			
Conductivity:	1000 mS/cm					
UV:	I1 =	260	I2 = 240			
RI:						
Last sample:	C14 L10					
Elution:	V injected:	1,5 BV				
	t injection:	25 min				
	Flowrate:	3,6 BV/h				
	Flow direction:	bottom to top				
	Autosampler:	t initial:	333 s			
		t valve on :	120 s			
		t valve off:	10 s			
Last sample:	C14 E9					
Desorption 1	V injected:	2,5 BV				
	t injection:	25 min				
	Flowrate:	6 BV/h				
	Flow direction:	top to bottom				
	Autosampler:	t initial:	200 s			
		t valve on :	120 s			
		t valve off:	10 s			
Conductivity:	1000 mS/cm					
UV:	I1 =	260	I2 = 240			
RI:						
Last sample:	C14 D1 10					
Desorption 2	V injected:	2,5 BV				
	t injection:	25 min				
	Flowrate:	6 BV/h				
	Flow direction:	top to bottom				
	Autosampler:	t initial:	200 s			
		t valve on :	120 s			
		t valve off:	10 s			
Conductivity:	1000 mS/cm					
UV:	I1 =	260	I2 = 240			
RI:						
Last sample:	C14 D2 10					
Regeneration:	V injected:	1 BV				
	t injection:	25 min				
	Flowrate:	2,4 BV/h				
	Flow direction:	top to bottom				
	Autosampler:	t initial:	250 s			
		t valve on :	120 s			
t valve off:		10 s				
Last sample:	C14 RE 7					

Table XXXIX C15 Parameters

Date:	13.2.2023			
Aim:	Fe-solution test, feed 0,5 BV			
Experiment:	C15			
Column:	Old			
Loading:	V injected:	0,5 BV		
	t injection:	5 min		
	Flowrate:	6 BV/h		
	Flow direction:	bottom to top		
Autosampler:	t initial:			
	t valve on :	no samples		
	t valve off:			
	Conductivity:	1000 mS/cm		
	UV:	l1 =	350	l2 = 240
	RI:			
	Last sample:			
Desorption 2:	V injected:	4 BV		
0,4 M K-oxalate	t injection:	40 min		
	Flowrate:	6 BV/h		
	Flow direction:	top to bottom		
Autosampler:	t initial:	0 s		
	t valve on :	120 s		
	t valve off:	10 s		
	Conductivity:	1000 mS/cm		
	UV:	l1 =	350	l2 = 240
	RI:			
	Last sample:			
Regeneration:	V injected:	2 BV		
	t injection:	20 min		
	Flowrate:	6 BV/h		
	Flow direction:	top to bottom		
Autosampler:	t initial:			
	t valve on :	no samples		
	t valve off:			
	Conductivity:	1000 mS/cm		
	UV:	l1 =	350	l2 = 240
	RI:			
	Last sample:			

Table XL C16 Parameters

Date:	13.2.2023				
Aim:	Fe-solution test, feed 1 BV				
Experiment:	C16				
Column:	Old				
Loading:	V injected:	1 BV			
	t injection:	10 min			
	Flowrate:	6 BV/h			
	Flow direction:	bottom to top			
Autosampler:	t initial:				
	t valve on :			no samples	
	t valve off:				
	Conductivity:	1000 mS/cm			
UV:	I1 =	350	I2 =	240	
RI:					
Last sample:					
Desorption 2:	V injected:	4 BV			
0,4 M K-oxalate	t injection:	40 min			
	Flowrate:	6 BV/h			
	Flow direction:	top to bottom			
Autosampler:	t initial:	0 s			
	t valve on :	120 s			
	t valve off:	10 s			
	Conductivity:	1000 mS/cm			
UV:	I1 =	350	I2 =	240	
RI:					
Last sample:					
Regeneration:	V injected:	2 BV			
	t injection:	20 min			
	Flowrate:	6 BV/h			
	Flow direction:	top to bottom			
Autosampler:	t initial:				
	t valve on :			no samples	
	t valve off:				
	Conductivity:	1000 mS/cm			
UV:	I1 =	350	I2 =	240	
RI:					
Last sample:					

Table XLI C17 Parameters

Date:	13.2.2023			
Aim:	Fe-solution test, feed 1,5 BV			
Experiment:	C17			
Column:	Old			
Loading:	V injected:	1,5 BV		
	t injection:	15 min		
	Flowrate:	6 BV/h		
	Flow direction:	bottom to top		
Autosampler:	t initial:			
	t valve on :	no samples		
	t valve off:			
	Conductivity:	1000 mS/cm		
	UV:	l1 =	350	l2 = 240
	RI:			
	Last sample:			
Desorption 2:	V injected:	4 BV		
0,4 M K-oxalate	t injection:	40 min		
	Flowrate:	6 BV/h		
	Flow direction:	top to bottom		
Autosampler:	t initial:	0 s		
	t valve on :	120 s		
	t valve off:	10 s		
	Conductivity:	1000 mS/cm		
	UV:	l1 =	350	l2 = 240
	RI:			
	Last sample:			
Regeneration:	V injected:	2 BV		
	t injection:	20 min		
	Flowrate:	6 BV/h		
	Flow direction:	top to bottom		
Autosampler:	t initial:			
	t valve on :	no samples		
	t valve off:			
	Conductivity:	1000 mS/cm		
	UV:	l1 =	350	l2 = 240
	RI:			
	Last sample:			

Table XLII C18 Parameters

Date:	13.2.2023			
Aim:	Fe-solution test, feed 4,5 BV			
Experiment:	C18			
Column:	Old			
Loading:	V injected:	4,5 BV		
	t injection:	45 min		
	Flowrate:	6 BV/h		
	Flow direction:	bottom to top		
Autosampler:	t initial:			
	t valve on :	no samples		
	t valve off:			
	Conductivity:	1000 mS/cm		
UV:	I1 =	350	I2 =	240
	RI:			
	Last sample:			
Desorption 2:	V injected: 4 BV			
0,4 M K-oxalate	t injection: 40 min			
	Flowrate: 6 BV/h			
	Flow direction: top to bottom			
Autosampler:	t initial:	0 s		
	t valve on :	120 s		
	t valve off:	10 s		
	Conductivity:	1000 mS/cm		
UV:	I1 =	350	I2 =	240
	RI:			
	Last sample:			
Regeneration:	V injected: 2 BV			
	t injection: 20 min			
	Flowrate: 6 BV/h			
	Flow direction: top to bottom			
Autosampler:	t initial:			
	t valve on :	no samples		
	t valve off:			
	Conductivity:	1000 mS/cm		
UV:	I1 =	350	I2 =	240
	RI:			
	Last sample:			

Table XLIII C19 Parameters

Date:	13.2.2023			
Aim:	Fe-solution test, feed 6 BV			
Experiment:	C19			
Column:	Old			
Loading:	V injected:	6 BV		
	t injection:	60 min		
	Flowrate:	6 BV/h		
	Flow direction:	bottom to top		
Autosampler:	t initial:			
	t valve on :	no samples		
	t valve off:			
	Conductivity:	1000 mS/cm		
UV:	I1 =	350	I2 =	240
RI:				
Last sample:				
Desorption 2:	V injected: 4 BV			
0,4 M K-oxalate	t injection: 40 min			
	Flowrate: 6 BV/h			
	Flow direction: top to bottom			
Autosampler:	t initial:	0 s		
	t valve on :	120 s		
	t valve off:	10 s		
	Conductivity:	1000 mS/cm		
UV:	I1 =	350	I2 =	240
RI:				
Last sample:				
Regeneration:	V injected: 2 BV			
	t injection: 20 min			
	Flowrate: 6 BV/h			
	Flow direction: top to bottom			
Autosampler:	t initial:			
	t valve on :	no samples		
	t valve off:			
	Conductivity:	1000 mS/cm		
UV:	I1 =	350	I2 =	240
RI:				
Last sample:				

Table XLIV C20 Parameters

Date:	30.1.2023					
Aim:	TP260 MDS resin, SMB settings, 100 % multi metal solution					
Experiment:	C20					
Column:	Old					
Loading:	V injected:	2,5 BV				
	t injection:	25 min				
	Flowrate:	6 BV/h				
	Flow direction:	bottom to top				
	Autosampler:	t initial:	200 s			
		t valve on :	120 s			
		t valve off:	10 s			
	Conductivity:	1000 mS/cm				
	UV:	l1 =	260	l2 =	240	
	RI:					
Last sample:	C20 L10					
Elution:	V injected:	1,5 BV				
	t injection:	25 min				
	Flowrate:	3,6 BV/h				
	Flow direction:	bottom to top				
	Autosampler:	t initial:	0 s			
		t valve on :	120 s			
		t valve off:	10 s			
	Last sample:	C20 E9				
Desorption 1	V injected:	4 BV				
	t injection:	40 min				
	Flowrate:	6 BV/h				
	Flow direction:	top to bottom				
	Autosampler:	t initial:	0 s			
		t valve on :	120 s			
		t valve off:	10 s			
	Conductivity:	1000 mS/cm				
	UV:	l1 =	260	l2 =	240	
	RI:					
Last sample:	C20 D1 8					
Desorption 2	V injected:	4 BV				
	t injection:	40 min				
	Flowrate:	6 BV/h				
	Flow direction:	top to bottom				
	Autosampler:	t initial:	0 s			
		t valve on :	120 s			
		t valve off:	10 s			
	Conductivity:	1000 mS/cm				
	UV:	l1 =	260	l2 =	240	
	RI:					
Last sample:	C20 D2 14					
Regeneration:	V injected:	2 BV				
	t injection:	25 min				
	Flowrate:	9,6 BV/h				
	Flow direction:	top to bottom				
	Autosampler:	t initial:	0 s			
		t valve on :	120 s			
		t valve off:	10 s			
Last sample:	C20 RE 8					

Table XLV C21 Parameters

Date:	30.1.2023					
Aim:	TP260 MDS resin, SMB settings, 50 % multi metal solution					
Experiment:	C21					
Column:	Old					
Loading:	V injected:	2,5 BV				
	t injection:	25 min				
	Flowrate:	6 BV/h				
	Flow direction:	bottom to top				
	Autosampler:	t initial:	200 s			
		t valve on :	120 s			
		t valve off:	10 s			
	Conductivity:	1000 mS/cm				
	UV:	I1 =	260	I2 = 240		
	RI:					
Last sample:	C21 L10					
Elution:	V injected:	1,5 BV				
	t injection:	25 min				
	Flowrate:	3,6 BV/h				
	Flow direction:	bottom to top				
	Autosampler:	t initial:	0 s			
		t valve on :	120 s			
		t valve off:	10 s			
	Last sample:	C21 E12				
Desorption 1	V injected:	4 BV				
	t injection:	40 min				
	Flowrate:	6 BV/h				
	Flow direction:	top to bottom				
	Autosampler:	t initial:	0 s			
		t valve on :	120 s			
		t valve off:	10 s			
	Conductivity:	1000 mS/cm				
	UV:	I1 =	260	I2 = 240		
	RI:					
Last sample:	C21 D1 18					
Desorption 2	V injected:	4 BV				
	t injection:	40 min				
	Flowrate:	6 BV/h				
	Flow direction:	top to bottom				
	Autosampler:	t initial:	0 s			
		t valve on :	120 s			
		t valve off:	10 s			
	Conductivity:	1000 mS/cm				
	UV:	I1 =	260	I2 = 240		
	RI:					
Last sample:	C21 D2 14					
Regeneration:	V injected:	2 BV				
	t injection:	25 min				
	Flowrate:	9,6 BV/h				
	Flow direction:	top to bottom				
	Autosampler:	t initial:	0 s			
		t valve on :	120 s			
		t valve off:	10 s			
Last sample:	C21 RE 8					

